Journal of Hydrology: Regional Studies 59 (2025) 102375

Contents lists available at ScienceDirect

Journal of Hydrology: Regional Studies

journal homepage: www.elsevier.com/locate/ejrh

Glacier meltwater contribution to river runoff in Western Mongolia

Purevdagva Khalzan [a,b], Sanjar Sadyrov [c,d], Akiko Sakai [b], Kenji Tanaka [d], Koji Fujita [b,*]

[a] Information and Research Institute of Meteorology Hydrology and Environment, Ulaanbaatar, 15160, Mongolia
[b] Graduate School of Environmental Studies, Nagoya University, Chikusa-ku, Nagoya, 464-8601, Japan
[c] Mountain Societies Research Institute, University of Central Asia, Bishkek, 720001, Kyrgyzstan
[d] Disaster Prevention Research Institute, Kyoto University, Uji, 611-0011, Japan

ARTICLE INFO

Dataset link: https://doi.org/10.5281/zenodo.14729735, https://cds.climate.copernicus.eu/, https://doi.org/10.5066/F7DF6PQS

Keywords:
Glacier meltwater
River runoff
Arid terrain
Mongolia

ABSTRACT

Study regions: Three river basins in western Mongolia (Khovd, Uvs, and Zavkhan).
Study focus: Water resources in Mongolia, which have been poorly studied to date, are limited and unevenly distributed, with the contribution of glacier meltwater being unknown. We simulated the runoff in three river basins in western Mongolia that receive glacier meltwater. ERA5 reanalysis data were evaluated using observations at 28 meteorological stations, and then the glacier meltwater and river runoff were simulated using statistically downscaled ERA5 reanalysis data and three models: an energy-mass-balance model for glaciers, a land-surface process model for ice-free terrain, and a river runoff model to combine the runoff from the two terrains. The simulated runoffs are validated with observations at 34 hydrological stations.
New hydrological insights for the region: The glacier meltwater contribution, which is first quantitatively evaluated, is substantial in the Khovd River basin, occurs only in some sub-basins of the Uvs Lake basin, and is negligible in the Zavkhan River basin. The glacier-free simulation indicates that, if glaciers were to disappear, river runoff would significantly decrease during the summer, with the peak flow shifting 1–2 months earlier compared to the present day. The glacier meltwater contribution to river runoff exhibits a nonlinear relationship with the glacier area contribution, which is much greater than that found in a previous study for Tien Shan, suggesting that shrinking ice mass would supply larger amounts of water. Analyses of correlation and extremes suggest that runoff from glacierized catchments responds differently than runoff from glacier-free terrains and thus would compensate for a water deficit caused by a warm and dry environment by supplying glacier meltwater, and vice versa.

1. Introduction

Mongolia, an inland country in Northeast Asia (Fig. 1), is isolated from the ocean (Sato et al., 2007; Antokhina et al., 2019). According to the Köppen–Geiger climate classification map, the mountain regions of northwestern Mongolia are polar and tundra zones, whereas the lowland regions are arid and desert zones (Kottek et al., 2006). The climate of Mongolia is characterized by a wide range of temperatures and low precipitation (Batsukh et al., 2008; Munkhbat et al., 2022).

Mongolia's total water resource is estimated to be about 600 km^3, with 89% of this water being stored in 3500 lakes, 5.5% in 3800 rivers, 3.5% in 560 glaciers, and 2.0% as groundwater (Garmaev et al., 2019). The high mountain ranges in northwestern Mongolia produce 70% of Mongolia's surface water (Batsukh et al., 2008). Glaciers are distributed across the 42 mountain massifs in the

* Corresponding author.
E-mail address: cozy@nagoya-u.jp (K. Fujita).

https://doi.org/10.1016/j.ejrh.2025.102375
Received 4 November 2024; Received in revised form 4 April 2025; Accepted 4 April 2025
Available online 8 May 2025
2214-5818/

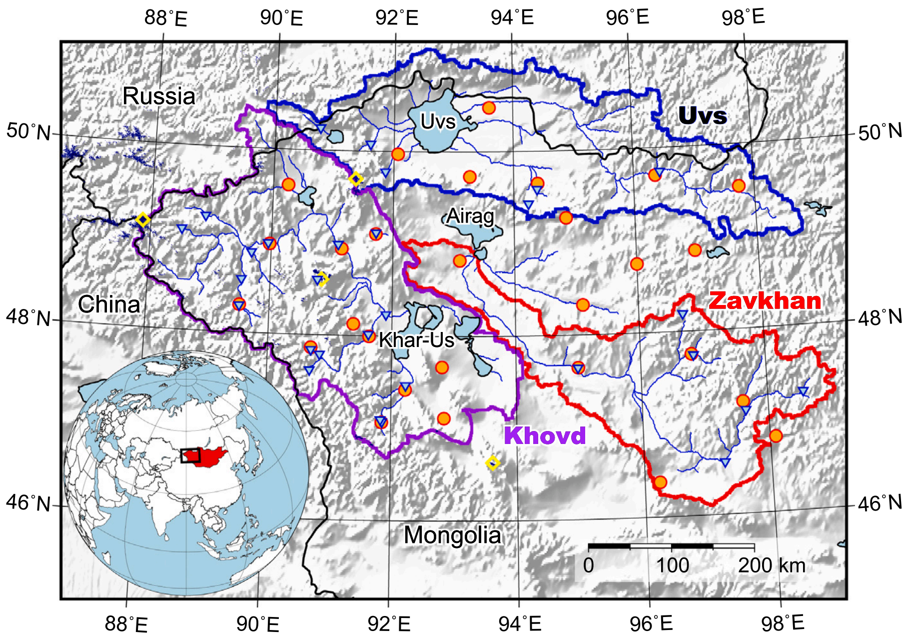

Fig. 1. Studied basins in western Mongolia (inset map). Purple, blue, and red polygons denote the Khovd River, Uvs Lake, and Zavkhan River basins, respectively. Blue lines, dark and light blue shadings denote rivers from the HydroSHEDS database (Lehner and Grill, 2013), glaciers from the GAMDAM glacier inventory (Nuimura et al., 2015; Sakai, 2019), and lakes, respectively. Khar-Us, Uvs, and Airag are the terminal lakes of the basins. Light blue triangles and orange circles denote hydrological and meteorological stations, respectively, whose details are available in Figure S1 and Tables 1 and 2. Open yellow diamonds denote the glaciers studied in a previous study (Khalzan et al., 2022) and their precipitation parameters are used in this study.

Mongolian Altai Mountains (Batimaa et al., 2011). In 2016 the total glacier area was 334 km^2 (627 glaciers), as inferred from Landsat −8 and Sentinel-2 image analysis, with 206 of these glaciers exhibiting a 43% reduction in glacier area between 1990 and 2016 (Pan et al., 2018). Ongoing fluctuations in the size of mountain glaciers, which may directly affect water resources and flow patterns, represent a crucial aspect of the hydrological systems within the watersheds of the Mongolian Altai Mountains. Consequently, climate change may reshape water resources by impacting glacier mass balances, thereby influencing regional development (Orkhonselenge and Harbor, 2018).

Few studies have examined glaciers and glacier-fed rivers in Mongolia. The first glacier-related study in Mongolia assessed the total glacier volume, which was estimated to be 62.8 km^3 (Dashdeleg et al., 1983). Century-scale changes in glacier size have been reported for glaciers in the Turgen Mountains (Kamp et al., 2013). Multi-decadal glacier inventories have been created for 1990, 2000, and 2010 (Kamp and Pan, 2015), with glacier recession then analyzed from these inventories (Pan et al., 2018). In situ glacier monitoring has been conducted for Potanin Glacier since 2003 (Kadota and Davaa, 2007; Kadota et al., 2011; Konya et al., 2010), and long-term annual mass balances have been reconstructed using energy-mass-balance models (Zhang et al., 2017; Khalzan et al., 2022). Davaa (2010) reported that the mean annual runoff for rivers originating from the Altai Mountains has increased by 15%–35% during the past 30–70 years, and proposed that the increased runoff was due to increased glacier melting. Pan et al. (2019) estimated the contribution of glacier meltwater (GMW) to river runoff in the upper Khovd River basin to be 8%–18% by assuming a simple mass-balance gradient and equilibrium line altitude (ELA), although the results were not validated and observational data were not considered. In a six-day observational study of the Tsambagarav Massif, Bantcev et al. (2019) estimated the contribution of GMW to river flow to be 20%–30%.

Previous studies of river runoff in western Mongolia have made estimates based on simple assumptions or short observational periods. No estimates have been made over the scale of large basins in the region or over multiple decades. This study aims to quantitatively evaluate the contribution of GMW to river runoff in western Mongolia using physically based models of glaciers and land-surface processes.

2. Data and methods

2.1. Target basins and data

We performed runoff simulations for the Khovd River, Uvs Lake, and Zavkhan River basins in western Mongolia (Fig. 1). The Khovd River basin, in westernmost Mongolia, is the most glacierized basin, with its runoff originating in the Altai Mountains and flowing into Khar-Us Lake (Dgebuadze et al., 2014; Syromyatina et al., 2015). The basin covers 57,000 km^2 and is monitored by 17 hydrological stations and 12 meteorological stations. The Uvs Lake basin, which is located in the northern part of western Mongolia

Table 1
Overview of the 30 hydrological stations in western Mongolia. A_{glc} denotes glacier area ratio.

Station name	Code	Large basin	Longitude (°E)	Latitude (°E)	Catchment area (km^2)	Glacier area (km^2)	A_{glc} (%)
Tsagaan Tsengel	TsT	Khovd	88.517	49.092	586.2	71.44	12.2
Sogoog Khokhkhotol	SoK	Khovd	88.899	49.244	1828.8	2.29	1.25×10^{-1}
Kharbut Altai	KhA	Khovd	89.513	48.292	3127.0	0.00	0.00
Sagsai Buyant	SaB	Khovd	89.534	48.578	4681.0	20.69	4.42×10^{-1}
Turgan Sagsai	TuS	Khovd	89.680	48.874	3235.6	12.70	3.93×10^{-1}
Khovd Ulgii	KhU	Khovd	89.948	48.979	25 513.9	202.66	7.94×10^{-1}
Khovd Bayannuur	KhB	Khovd	91.101	48.986	39 977.1	258.08	6.46×10^{-1}
Ulaan am Erdeneburen	UaE	Khovd	90.773	48.601	22.1	2.24	10.1
Namir Omnogovi	NaO	Khovd	91.719	49.118	583.24	9.2	1.59
Chigertei Deluun	ChD	Khovd	90.697	47.839	2107.01	5.0	2.38×10^{-1}
Gantsmod Deluun	GaD	Khovd	90.684	47.619	3650.7	4.40	1.20×10^{-1}
Buyant Deluun	BuD	Khovd	90.840	47.790	1146.7	1.43	1.25×10^{-1}
Buyant Khovd	BuK	Khovd	91.621	48.015	7132.3	9.74	1.37×10^{-1}
Khovd Myangad	KhM	Khovd	91.900	48.233	55 673.0	329.29	5.91×10^{-1}
Dundtsenkher Monkhkhairkhan	DuM	Khovd	91.857	47.071	2030.7	27.18	1.34
Doloonnuur Monkhkhairkhan	DoM	Khovd	91.831	47.093	1567.0	24.85	1.59
Togrog Mankhan	ToM	Khovd	92.229	47.466	5532.9	22.74	4.11×10^{-1}
Kharig Sagil	KhS	Uvs	90.757	50.240	1563.0	17.26	1.10
Turgen Turgen	TuT	Uvs	91.606	50.077	993.1	7.89	7.94×10^{-1}
Kharkhiraa Tarialan	KhT	Uvs	91.861	49.780	886.9	34.77	3.92
Khangiltsag Tsagaankhairhan	KgT	Uvs	94.242	49.431	494.7	0.00	0.00
Baruunturuun Baruunturuun	BaB	Uvs	94.389	49.588	1000.0	0.00	0.00
Tes Bayan Uul	TbU	Uvs	96.440	49.742	12 470.2	0.00	0.00
Yaruu Yaruu	YaY	Zavkhan	96.710	48.190	425.3	0.00	0.00
Chigestei Uliastai	ChU	Zavkhan	96.849	47.740	1661.2	0.69	4.15×10^{-2}
Bogd Uliastai	BoU	Zavkhan	96.850	47.740	2715.6	0.38	1.41×10^{-2}
Shar Us Gurvanbulag	SuG	Zavkhan	98.565	47.283	1039.9	0.00	0.00
Buyant Otgon	BuO	Zavkhan	97.639	47.118	8666.9	0.06	7.26×10^{-4}
Zavkhan Guulin	ZaG	Zavkhan	97.267	46.567	11 908.2	0.18	1.52×10^{-3}
Zavkhan Dorvoljin	ZaD	Zavkhan	94.993	47.644	38 012.1	0.18	4.80×10^{-4}

and is 5700 km^2 in size, is designated as a natural world heritage site (Grunert et al., 2000). Glaciers occur in the Turgen-Kharkhiraa Mountains in the western part of the basin. The basin includes six hydrological and six meteorological stations. The drainage systems within the Zavkhan River basin originate mainly in the Khangai Mountains and flow into Airag Lake (Ochir et al., 2013). The 98,000-km^2 basin is monitored by seven hydrological and five meteorological stations.

In this study, we simulated and validated the daily runoff recorded at 30 hydrological stations for the period 2000–2020 (Figures 1 and S1a). We used the air temperature and precipitation data recorded at 28 meteorological stations in and around the Khovd River, Uvs Lake, and Zavkhan River basins to confirm and calibrate the ERA5 data for the period 1990–2020 (Figures 1 and S1b). We also used the precipitation parameters that were determined in this study and a previous study of four glaciers in the Mongolian Altai Mountains (Khalzan et al., 2022) to calibrate the ERA5 precipitation. Additional details on the hydrological and meteorological stations used in this study and the glaciers studied by Khalzan et al. (2022) are summarized in Tables 1 and 2.

Fig. 2 shows an outline of the data preprocessing and simulation in this study. We first confirmed the reproducibility of the ERA5 temperature and calibrated the ERA5 precipitation values using the observed values at 28 meteorological stations (Hersbach et al., 2020). We then statistically downscaled the ERA5 data from 0.25° to 5-arc-min (~10-km) resolution as the meteorological forcing data for the models. We estimated the meteorological variables via the inverse distance weighing (IDW) method, with an effective radius of 0.2°. The air temperature was calibrated at sea level with the temperature lapse rate (6.0 °C km^{-1}) before and after the spatial downscaling. The downward longwave radiation depends on air temperature via the Stefan–Boltzmann equation. A calibration parameter, such as atmospheric emissivity (ε_a), can therefore be estimated as a function of air temperature (T_a, °C) and downward longwave radiation (R_{Ld}, W m^{-2}) as follows:

$$\varepsilon_a = \frac{R_{Ld}}{\sigma(T_a + 273.15)^4}, \tag{1}$$

where σ is the Stefan–Boltzmann constant (5.67×10^{-8} W m^{-2} K^{-4}). The estimated atmospheric emissivity was also spatially downscaled, and the downscaled downward longwave radiation was then calculated from the downscaled air temperature via Eq. (1).

2.2. Models

We adopted three models to simulate the river runoff in the three river basins in western Mongolia: (1) a land-surface model (Simple Biosphere including Urban Canopy model, SiBUC) to determine the energy and water balance over the off-glacier terrain, (2) an energy-mass-balance model (GLacIer energy Mass Balance model, GLIMB) to estimate the amount of GMW, and (3) a river

Table 2
Overview of the 28 meteorological stations and four glaciers in western Mongolia. SAT and APR denote mean summer temperature and annual precipitation, respectively. r_p denotes the precipitation ratio to calibrate the ERA5 precipitation. Data of four glaciers are of Khalzan et al. (2022).

Station name	Code	Large basin	Longitude (°E)	Latitude (°E)	Elevation (m a.s.l.)	SAT (°C)	APR (mm)	r_p
Nogoonnuur	NG	Khovd	90.248	49.614	1474	17.26 ± 0.84	85 ± 26	0.344
Ulgii	UL	Khovd	89.970	48.970	1720	16.46 ± 0.89	117 ± 29	0.594
Yalalt	YL	Khovd	89.515	48.299	2137	12.26 ± 0.81	143 ± 31	0.471
Khar-Us	KU	Khovd	91.718	49.104	1589	16.29 ± 0.93	139 ± 44	0.665
Bayannuur	BY	Khovd	91.162	48.939	1333	19.10 ± 0.78	94 ± 25	0.520
Deluun	DL	Khovd	90.697	47.863	2150	13.31 ± 0.91	105 ± 27	0.511
Dund-Us	DU	Khovd	91.373	48.126	1711	17.04 ± 0.78	163 ± 43	0.422
Khovd	KV	Khovd	91.633	47.996	1405	14.51 ± 0.90	130 ± 35	0.680
Chandmani	CD	Khovd	92.813	47.664	1661	17.58 ± 1.04	150 ± 56	0.485
Mankhan	MK	Khovd	92.224	47.420	1352	19.85 ± 0.85	76 ± 25	0.393
Zereg	ZR	Khovd	92.844	47.111	1152	21.40 ± 1.28	81 ± 34	0.275
Monkhkhairkhan	MO	Khovd	91.853	47.065	2093	14.58 ± 0.97	145 ± 18	0.537
Ulaangom	UG	Uvs	92.069	49.972	939	18.84 ± 0.93	147 ± 54	0.503
Tes	TS	Uvs	93.601	50.476	799	19.44 ± 0.93	129 ± 39	0.575
Malchin	MC	Uvs	93.269	49.729	1393	16.59 ± 0.92	263 ± 79	0.749
Baruunturuun	BT	Uvs	94.400	49.650	1234	17.58 ± 1.10	245 ± 62	0.750
Bayan-Uul	BU	Uvs	96.363	49.700	1420	15.60 ± 1.03	195 ± 40	0.626
Chandagat	CG	Uvs	97.748	49.535	1744	13.40 ± 1.05	228 ± 69	0.698
Ondorkhangai	OK	NA	94.861	49.271	1863	14.38 ± 0.69	190 ± 49	0.494
Nomrog	NR	NA	96.962	48.871	1847	13.75 ± 1.01	180 ± 52	0.724
Tsetsen-Uul	TU	NA	96.004	48.748	1927	12.63 ± 1.18	238 ± 52	0.614
Zavkhanmandal	ZM	NA	95.099	48.325	1442	17.82 ± 0.69	138 ± 37	0.843
Zavkhan	ZH	Zavkhan	93.103	48.822	1049	20.89 ± 0.99	70 ± 30	0.618
Dorvoljin	DR	Zavkhan	94.999	47.647	1391	19.26 ± 1.10	96 ± 45	0.732
Uliastai	US	Zavkhan	96.820	47.750	1391	15.59 ± 1.23	219 ± 72	0.717
Otgon	OT	Zavkhan	97.605	47.210	2156	12.56 ± 1.10	161 ± 51	0.618
Altai	AT	Zavkhan	96.238	46.378	2180	14.29 ± 1.12	180 ± 46	0.654
Bayanbulag	BB	NA	98.087	46.812	2257	12.55 ± 1.13	146 ± 50	0.510
Potanin Glacier	PT	Khovd	87.866	49.154	3650	0.00 ± 0.85	621 ± 58	0.650
Tsambagarav Glacier	TB	Khovd	90.841	48.603	3707	−0.19 ± 0.89	248 ± 39	0.670
Turgen Glacier	TG	Uvs	91.368	49.697	3360	1.84 ± 1.01	855 ± 93	0.920
Sutai Glacier	ST	NA	93.615	46.629	3976	0.11 ± 0.92	190 ± 39	0.660

routing model (Rainfall Runoff Inundation, RRI) to combine the runoff from the SiBUC and GLIMB models. This hybrid approach allows us to account for the sub-grid heterogeneity in glacier and land surface characteristics while maintaining computational feasibility for the large study region (Sadyrov et al., 2024).

2.2.1. Land-surface model: SiBUC

We adopted SiBUC, a land-surface model that calculates the water and energy balance in a gridded system (Tanaka, 2005), to simulate the land-surface processes in each basin. The SiBUC model, which is based on the SiB (Sellers et al., 1986) and SiB2 (Sellers et al., 1996) models, calculates the surface processes for several mosaic schemes, such as green areas, water bodies, and urban areas. Here we briefly describe the surface processes over the off-canopy bare ground, which is the major surface condition in western Mongolia. See Tanaka (2005) for further details of the SiBUC model. The ground surface temperature (T_g) is estimated by a submodel for the green area to determine the surface flux, and a force-restore model then calculates heat transfer in the soil (Deardorff, 1977). The heat conduction equation is analytically solved by assuming a periodic forcing, and the periodic ground heat flux and deep soil temperature (T_d) are then parameterized. This approach allows a feasible representation of temperature dynamics. The governing equations for the ground surface and soil temperatures are as follows:

$$C_g \frac{\partial T_g}{\partial t} = Rn_g + H_S + H_L - \omega C_g (T_g - T_d), \tag{2}$$

where C_g is the heat capacity for ground soil; Rn_g is the net radiation absorbed at the ground; and H_S and H_L are the sensible and latent heat fluxes, respectively. The absorbed net radiation, which consists of shortwave and longwave radiation, is expressed as follows:

$$Rn_g = (1 - \alpha_g) R_{Sd} + R_{Ld} + \epsilon_g \sigma (T_g + 273.15)^4, \tag{3}$$

where α_g is the surface albedo; R_{Sd} and R_{Ld} are the downward shortwave and longwave radiation, respectively; and ϵ_g is the emissivity of the surface terrain.

The governing equation for interception water that accumulates on the ground (M_g) is as follows:

$$\frac{\partial M_g}{\partial t} = P - (P_c - D_c) - P_i - D_g - \frac{E_{wg}}{\rho_w}, \tag{4}$$

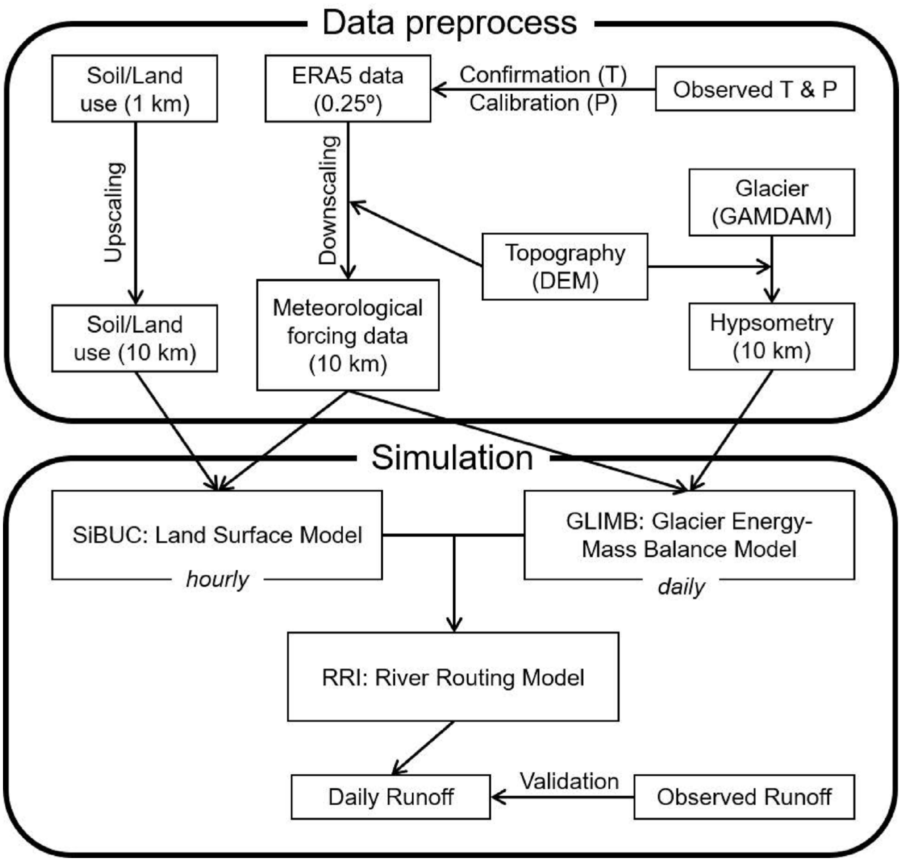

Fig. 2. Flowchart of the study. T and P denote air temperature and precipitation, respectively.

where P is precipitation; $(P_c - D_c)$ is the water captured by the canopy, which is expressed by the precipitation on the canopy (P_c) and the water drainage rate from the canopy (D_c); P_i is the infiltration of precipitation into the upper soil layer; D_g is the rate of water drainage from the surface; E_{wg} is evaporation ($\mathrm{kg\ m^{-2}\ s^{-1}}$); and ρ_w is the density of water ($1000\ \mathrm{kg\ m^{-3}}$).

The heat and moisture transfers in the soil are calculated using a three-layer isothermal model that considers hydraulic diffusion and the gravitational drainage of water. The total runoff from green areas (R_{grd}) is determined by summing the surface runoff (D_g) and baseflow (Q_b), which is equivalent to the gravitational drainage from the recharge layer.

The land-cover type affects the energy, radiation, and water budgets. The SiBUC model incorporates a mosaic approach to reflect mixtures of different land-cover types (Tanaka, 2005). The land-surface parameters used in this study include the land-cover fractions dataset (Loveland et al., 2000). The soil parameters were identified using the 1-km (30-arc-sec) ECOCLIMAP dataset (Champeaux et al., 2005). The GTOPO30 (30-arc-sec) dataset was used as the digital elevation model (DEM). All the model parameters were determined using land-surface products, thereby eliminating the need for calibration. The soil characteristic parameters in the SiBUC model are based on (Cosby et al., 1984). The parameters at a 1-km resolution were averaged to a 5-arc-min (~10-km) grid resolution for the SiBUC simulation.

2.2.2. Glacier energy-mass-balance model: GLIMB

Although the SiBUC model calculates snow processes (snow accumulation and melting) over the terrain, it does not consider glaciers, which can produce excess meltwater by ice ablation. We therefore adopted GLIMB, which was previously applied to glaciers in high mountain Asia (Fujita and Ageta, 2000; Fujita and Sakai, 2014), to incorporate glaciological processes into the overall scheme. The surface heat balance (Q_m) is calculated as follows:

$$Q_m = Rn_s + H_S + H_L - G_g, \tag{5}$$

where Rn_s is the net radiation absorbed at the glacier surface, whereby the albedo and surface temperature in Eq. (3) are replaced by those for the glacier surface (α_s and T_s, respectively), and G_g is the conductive heat flux into the glacier ice, which is determined from the temperature profile through the ice. Glacier runoff (R_{glc}) is calculated as follows:

$$R_{glc} = \frac{Q_m}{l_m} + P_r + \max\left[\frac{H_L}{l_e}, 0\right] - R_{ref}, \tag{6}$$

where l_m and l_e are the latent heat of ice melting and water evaporation, respectively; P_r is rainfall; and R_{ref} is refrozen water in the snow layer. Runoff from the glacier is input into the river system through a bucket model that includes two storages (Motoya and Kondo, 1999). Further details of the model can be found in Fujita and Ageta (2000) and Fujita and Sakai (2014).

GLIMB uses daily data as input and has been successful in simulating glacier mass balance and runoff under a variety of climates such as the central (Fujita et al., 2007), northern (Sakai et al., 2009, 2010), and southeastern (Zhang et al., 2016a) Tibet, Tien Shan (Sadyrov et al., 2024), and Patagonia (Minowa et al., 2023). GMW generation is more sensitive to elevation than to horizontal resolution of input variables. Therefore, the GLIMB model calculates glacier runoff at 50-m intervals in elevation. The hypsometry (area-elevation profile) of the glacier surface (a_{glc_z}, km^2) is summarized at a 5-arc-min grid (∼10-km) resolution using the GAMDAM glacier inventory (Nuimura et al., 2015; Sakai, 2019) and ASTER-GDEM3 (Tachikawa et al., 2011).

2.2.3. River runoff model: RRI

We adopted the RRI model, which is a two-dimensional (2-D) model that can simultaneously simulate river runoff and flood inundation (Sayama et al., 2012), to integrate the runoff from the on- and off-glacier terrains and then calculate the river runoff. The RRI model is designed to capture the spatial and temporal variability of runoff and inundation, whereby it considers the effects of both the slope and surface roughness. Note that the model deals with slopes and river channels separately. At a given grid cell in which a river channel is located, the channel is discretized as a single vector along the centerline of the overlying slope grid cell. The channel represents an extra flow path between grid cells lying over the actual river course. Lateral flows are simulated on slope cells (without a channel) on a 2-D basis.

The basin topography inputs, which include the void-filled DEM, a drainage direction map, and a flow accumulation map of the targeted hydrological stations for the RRI simulation, were extracted at a 30-arc-sec (∼1-km) resolution from the HydroSHEDS database (Lehner and Grill, 2013). A gridded rainfall dataset is generally used as input for the RRI model. We calculated an integrated runoff dataset at a 5-arc-min (∼10-km) resolution in our simulations as follows:

$$R_{x,y} = \frac{R_{grd} A_{grd} + \sum_z R_{glc_z} a_{glc_z}}{A_{grd} + \sum_z a_{glc_z}}, \tag{7}$$

where $R_{x,y}$ is the daily runoff depth (mm d^{-1}) at a given grid cell, R_{glc_z} is the daily runoff depth of glacier surface (mm d^{-1}) at a given elevation band (z, m above sea level), and A_{grd} is the area of the glacier-free terrain (km^2) in a 5-arc-min (∼10-km) grid cell. The daily runoff depth on- and off-glacier (R_{glc_z} and R_{grd_z}) are independently calculated by GLIMB and SiBUC. The RRI simulation were performed for the period 1999–2020, and then the first year (1999) output was omitted as a relaxation period.

To evaluate the simulations, we calculated the normalized Nash–Sutcliffe efficiency (E_{NNS}) of the simulated runoff using the daily runoff as follows:

$$\begin{aligned} E_{NS} &= 1 - \frac{\sum_d (R_{o_d} - R_{m_d})^2}{\sum_d (R_{o_d} - \overline{R_o})^2}, \\ E_{NNS} &= \frac{1}{2 - E_{NS}}, \end{aligned} \tag{8}$$

where E_{NS} is the Nash–Sutcliffe efficiency; R_{o_d} and R_{m_d} are the observed and simulated daily (d) runoffs, respectively; and $\overline{R_o}$ is the annual mean of the observed runoff (Nash and Sutcliffe, 1970). The efficiency, which ranges from 1 to $-\infty$, is then normalized to the range between 1 and 0 (Mathevet et al., 2006). For each station, E_{NNS} was calculated every year for the period 2000–2020, with its mean and standard deviation calculated for years with > 180 days of observed data.

3. Results

3.1. Performance of the ERA5 data

The 2-m air temperature at the elevation of each meteorological station was extracted from the pressure-level atmospheric air temperatures and geopotential heights in the ERA5 data to confirm the reproducibility of the ERA5 temperatures (Khalzan et al., 2022). Figure S2 shows the ERA5 and observed mean summer temperatures (June–August) for 1990–2020. The root mean square error (RMSE) exceeds 2 °C at two stations (MO and TU) and is <1 °C at 17 of the 28 meteorological stations. These RMSE results indicate that the ERA5 temperature data for western Mongolia are feasible for use in subsequent simulations.

The ERA5 summer precipitation, which are compared for 1990–2020, shows spatially variable biases (Fig. 3). We adopted the slope of the regression line with zero intercept as the precipitation parameter, which we then used to calibrate the ERA5 precipitation. We also included the precipitation parameters that were determined at four glaciers (Khalzan et al., 2022) to calculate the distribution of the precipitation parameter by the IDW method and then downscale the precipitation.

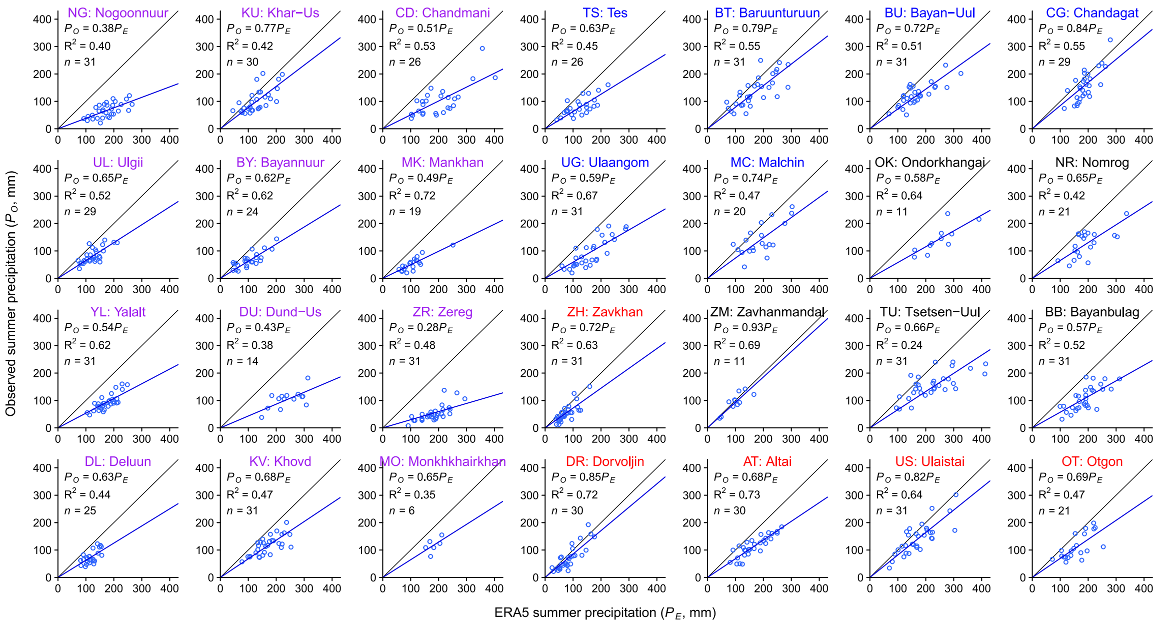

Fig. 3. Comparison of summer precipitations of ERA5 (P_E, horizontal axes) and observation (P_O, vertical axes) at the 28 meteorological stations in western Mongolia. Text colors of the station correspond to the large basins (Fig. 1).

3.2. Simulated runoff

Fig. 4 shows climatological means of observed and simulated runoff. Monthly time series for 2000–2020 are shown in Figures S3 and S4. As shown in Fig. 5a, the normalized Nash–Sutcliffe efficiency (E_{NNS}) is high in the Khovd River basin (0.725 ± 0.084, ranging between 0.618 and 0.894), moderate in the Uvs Lake basin (0.652 ± 0.092, ranging between 0.546 and 0.791), and lower in the Zavkhan River basin (0.559 ± 0.034, ranging between 0.503 and 0.603) (all the values are summarized in Table 3). E_{NNS} tends to be lower (<0.7) in the glacier-free basins, even though the seasonal patterns are generally reproduced. The monthly runoff time series (Figures S3 and S4) suggest that the observed period each year seems unnaturally short at the two stations with the lowest E_{NNS} (SuG and YaY). Figures S3 and S4 also suggest that the interannual variability in runoff seems to be well reproduced for the glacierized catchments, whereas it is poorly reproduced for the glacier-free catchments. The interannual variability in GMW is greater than that in runoff from the glacier-free catchment, and the precipitation parameter is a single value at each station (and then a spatially fixed value), such that the simulated interannual variabilities in runoff are basically due to the interannual variability in ERA5 precipitation. Furthermore, the winter reproducibility in small basins is generally poor because river freezing during winter is not considered in the models.

3.3. Contribution of glacier meltwater to river runoff

Figures 4, S3, and S4 show the contribution of GMW to runoff, which was independently calculated using the GLIMB and RRI models, and runoff in the case of no glaciers, for which runoff integration via Equation (7) was not performed. The seasonal patterns indicate a continuous increase in GMW from mid-May to early June that then drops to almost zero by November. Considering that the GMW contribution becomes more noticeable from June, the increase in river flow from April is directly caused by seasonal snowmelt at lower elevations. GMW seems to contribute to a maximum sustained river runoff from July to August, thereby producing an overall broader runoff pattern. Conversely, the simulation for a glacier-free environment shows a significant decrease in river runoff during summer, with flow peak occurring 1–2 months earlier than in the case with glaciers. Fig. 5b shows the spatial distribution of the GMW contribution (GMW to total runoff in %). The GMW contribution is large at the hydrological stations in the Khovd River basin, as Mongolian glaciers are located mainly in the Altai Mountains. The GMW in the western part of the Uvs Lake basin is from glaciers in the Turgen-Kharkhiraa Mountains (KhS, TuT, and KhT stations).

As a part of validation, we compared the simulated glacier mass balance (B_{sim}) with remotely sensed geodetic ones (B_{geod}), which were adopted from Hugonnet et al. (2021), for 652 glaciers in western Mongolia (Figure S5). Although the relationship between B_{sim} and B_{geod} is not that good, it does not stray too far from the one-to-one relationship. It appears that B_{sim} slightly overestimates the negative mass balance compared to B_{geod}. This suggests that the simulated meltwater from individual glaciers could be greater than in reality. However, the area weighted averages (black circle with error cross) seem consistent each other, suggesting that the simulated GMW would be plausible in the catchment scale.

Table 3
Observed and simulated river runoff at the 30 hydrological stations in western Mongolia. ANR, E_{NNS}, GMW, SAT, and APR denote annual mean runoff, normalized Nash–Sutcliffe efficiency, glacier meltwater, mean summer temperature, and annual precipitation, respectively. V_{glc} denotes glacier meltwater ratio in volume. Subscripts obs, sim, and ngl denote observation, simulation and simulation with no-glacier configuration, respectively.

Station code	ANR_{obs} (m^3 s^{-1})	ANR_{sim} (m^3 s^{-1})	E_{NNS}	GMW_{sim} (m^3 s^{-1})	V_{glc} (%)	ANR_{ngl} (m^3 s^{-1})	SAT (°C)	APR (mm)
TsT	9.76 ± 4.04	5.46 ± 0.57	0.78 ± 0.33	4.01 ± 0.59	73.27 ± 6.65	1.16 ± 0.33	5.57 ± 0.79	485 ± 43
SoK	4.06 ± 1.24	3.44 ± 0.53	0.62 ± 0.11	0.18 ± 0.03	5.34 ± 1.23	3.25 ± 0.53	7.84 ± 0.78	382 ± 44
KhA	2.98 ± 0.84	2.49 ± 0.37	0.67 ± 0.10	0.00	0.00	2.49 ± 0.37	8.42 ± 0.78	405 ± 39
SaB	15.77 ± 4.78	16.02 ± 1.70	0.76 ± 0.20	3.33 ± 0.37	20.99 ± 3.26	12.62 ± 1.71	9.05 ± 0.77	383 ± 39
TuS	2.53 ± 0.67	2.89 ± 0.25	0.62 ± 0.19	0.72 ± 0.08	25.01 ± 3.29	2.14 ± 0.24	9.90 ± 0.77	293 ± 40
KhU	59.49 ± 11.09	56.17 ± 6.56	0.89 ± 0.06	17.90 ± 2.47	32.25 ± 5.56	37.86 ± 6.69	9.72 ± 0.76	357 ± 38
KhB	63.44 ± 16.99	65.59 ± 6.95	0.86 ± 0.17	16.96 ± 2.22	26.13 ± 4.29	48.54 ± 7.16	10.81 ± 0.76	339 ± 39
UaE	0.34 ± 0.06	0.23 ± 0.06	0.78 ± 0.07	0.19 ± 0.06	83.31 ± 6.52	0.03 ± 0.01	3.35 ± 0.81	493 ± 73
NaO	1.58 ± 0.62	1.52 ± 0.30	0.68 ± 0.14	0.16 ± 0.05	10.88 ± 4.54	1.36 ± 0.32	9.64 ± 0.82	535 ± 79
ChD	3.40 ± 0.84	2.51 ± 0.37	0.70 ± 0.10	0.51 ± 0.07	20.60 ± 3.59	1.99 ± 0.35	8.92 ± 0.78	336 ± 33
GaD	3.35 ± 0.82	3.16 ± 0.44	0.70 ± 0.12	0.53 ± 0.07	17.10 ± 2.89	2.62 ± 0.42	8.91 ± 0.78	345 ± 35
BuD	1.71 ± 0.63	1.30 ± 0.12	0.67 ± 0.19	0.32 ± 0.05	24.80 ± 3.10	0.98 ± 0.10	9.63 ± 0.77	305 ± 34
BuK	7.67 ± 2.05	8.56 ± 0.99	0.67 ± 0.27	1.43 ± 0.18	16.84 ± 2.47	7.09 ± 0.94	10.20 ± 0.79	315 ± 35
KhM	85.83 ± 16.75	82.48 ± 8.29	0.87 ± 0.07	20.95 ± 3.00	25.59 ± 4.12	61.37 ± 8.32	11.35 ± 0.77	327 ± 37
DuM	1.81 ± 0.59	1.90 ± 0.15	0.71 ± 0.17	0.73 ± 0.10	38.17 ± 3.67	1.17 ± 0.10	8.25 ± 0.8	319 ± 45
DoM	1.08 ± 0.51	0.94 ± 0.07	0.71 ± 0.17	0.35 ± 0.05	36.63 ± 3.82	0.59 ± 0.05	7.99 ± 0.8	315 ± 44
ToM	3.38 ± 0.85	3.30 ± 0.26	0.632 ± 0.105	0.73 ± 0.10	22.19 ± 2.84	2.56 ± 0.23	10.89 ± 0.82	313 ± 47
KhS	3.04 ± 0.69	2.98 ± 0.42	0.732 ± 0.073	0.55 ± 0.13	18.93 ± 5.42	2.46 ± 0.45	10.40 ± 0.77	462 ± 57
TuT	2.30 ± 0.83	2.36 ± 0.50	0.682 ± 0.260	0.19 ± 0.05	8.45 ± 3.34	2.17 ± 0.52	10.73 ± 0.79	589 ± 82
KhT	4.60 ± 1.24	4.39 ± 0.75	0.791 ± 0.258	0.53 ± 0.15	12.73 ± 4.97	3.85 ± 0.81	9.05 ± 0.8	749 ± 97
KgT	0.91 ± 0.50	1.11 ± 0.28	0.547 ± 0.219	0.00	0.00	1.11 ± 0.28	12.93 ± 0.94	372 ± 66
BaB	1.89 ± 1.02	1.72 ± 0.45	0.546 ± 0.278	0.00	0.00	1.72 ± 0.45	14.70 ± 0.93	395 ± 70
TbU	14.38 ± 6.42	14.09 ± 2.19	0.61 ± 0.28	0.00	0.00	14.09 ± 2.19	13.30 ± 0.91	378 ± 59
YaY	2.33 ± 0.37	0.93 ± 0.23	0.53 ± 0.05	0.00	0.00	0.93 ± 0.23	12.41 ± 0.93	374 ± 66
ChU	2.84 ± 1.37	2.44 ± 0.64	0.57 ± 0.09	0.03 ± 0.01	1.41 ± 0.48	2.40 ± 0.64	10.65 ± 0.91	395 ± 70
BoU	8.47 ± 4.34	7.27 ± 1.95	0.56 ± 0.17	0.07 ± 0.02	1.02 ± 0.36	7.19 ± 1.95	11.01 ± 0.92	387 ± 70
SuG	1.02 ± 0.85	1.10 ± 0.14	0.50 ± 0.31	0.00	0.00	1.10 ± 0.14	10.33 ± 0.86	305 ± 61
BuO	7.29 ± 5.25	6.35 ± 0.94	0.60 ± 0.26	0.01 ± 0.00	0.14 ± 0.04	6.34 ± 0.94	9.92 ± 0.87	327 ± 56
ZaG	12.74 ± 6.36	7.27 ± 1.09	0.55 ± 0.11	0.01 ± 0.00	0.10 ± 0.03	7.26 ± 1.09	10.79 ± 0.88	303 ± 55
ZaD	20.07 ± 10.88	17.90 ± 3.11	0.60 ± 0.24	0.02 ± 0.01	0.12 ± 0.04	18.03 ± 3.12	14.03 ± 0.91	264 ± 53

Fig. 6 shows the relationships of runoff indices (GMW contribution, coefficient of variation (CV) of the annual runoff, and runoff coefficient (RC)) against the glacier area ratio at all stations (data listed in Tables 3 and S1). If the glaciers were in equilibrium (in terms of mass balance) and the amount of precipitation was constant at given elevation, then the GMW contribution should be either approximately equal to the glacier area ratio (plotted as the one-to-one line in Fig. 6a) or less due to evaporation. The power functional relationship in the figure suggests that glaciers at higher elevations receive much more precipitation and consequently provide more meltwater due to their long-lasting negative mass balance (Khalzan et al., 2022). Fig. 6b shows coefficient of variation (CV) of annual runoff, which is obtained by the standard deviation of annual runoff divided by its long-term mean (both for the 21 years), against the glacier area ratio. Observation-based (CV_{obs}) and simulated (CV_{sim}) CVs decrease with the glacier area ratio. A CV of the non-glacier configuration (CV_{ngl}) seems independent from the glacier area ratio (practically zero for all catchments). The difference between CV_{sim} and CV_{ngl} indicates the role of GMW for inter-annual variability of river runoff. Fig. 6c shows the runoff coefficient (RC), which is obtained by the area averaged runoff depth divided by annual precipitation, against the glacier area ratio. The large differences between RC_{sim} and RC_{ngl} along the glacier area ratio suggests that only 10% of precipitation could be available for the river runoff if no glacier exists due to the arid environment, and the large part of the river runoff is supplied as GMW in western Mongolia.

3.4. Controlling factors of glacier-affected river runoff

We simulated multiple basins with different glacier contributions, ranging from glacier-free basins to those with a glacier area ratio of up to 10% and a volume-based GMW contribution of 83% at Ulaan am Erdeneburen station (UaE). Here we investigate how these differences in glacier contribution affect the relationship between meteorological factors (temperature and precipitation) and annual fluctuations in river runoff by analyzing the correlations among these parameters and the impact of extreme events.

3.4.1. Interannual variability

We first obtained the annual mean of the mean summer temperature and annual amount of precipitation for each simulated basin from the ERA5-calibrated daily temperature and precipitation data. The number of grid cells of the targeted catchment (30-arc-sec or 1-km resolution) that were included in an input forcing grid cell (5-arc-min or 10-km resolution) were counted and then weighted during the averaging procedure. We then calculated the correlation coefficients between the meteorological forcing (mean summer temperature and annual precipitation) and the annual runoff. For the observational data, we selected the nearest meteorological

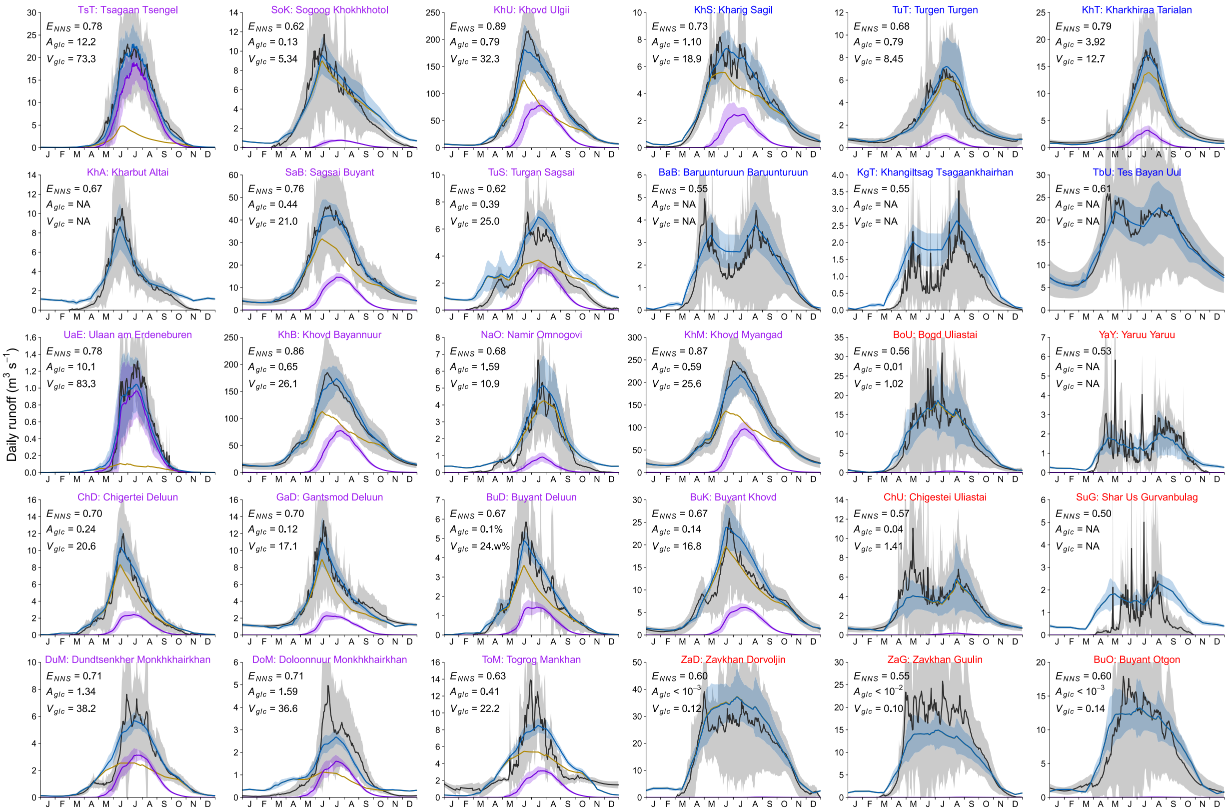

Fig. 4. Seasonal patterns of observational (black) and simulated (blue) daily runoff at the 30 hydrological stations in western Mongolia. Purple and brown lines denote glacier meltwater (GMW) and runoff without glacier configuration, respectively. E_{NNS}, A_{glc}, and V_{glc} denote the normalized Nash–Sutcliffe efficiency, glacier area ratio (%), and GMW contribution (%), respectively.

station for each hydrological station, and then obtained the correlation coefficients (Table S2). The corresponding meteorological and hydrological stations are also summarized in the table.

Fig. 7 shows that the glacier-free catchments do not exhibit a correlation between mean summer temperature or annual precipitation and river runoff. However, the runoff in the catchments where the GMW contribution is <20% shows highly negative correlations to mean summer temperature (Fig. 7a) and positive ones to annual precipitation (Fig. 7b), respectively. Increasing GMW contribution causes the correlations to increase toward positive correlations with mean summer temperature and to decrease toward no correlation with annual precipitation (Fig. 7a and b). The correlations among the observational data exhibit a similar relationship to that of the simulations with annual precipitation (Fig. 7d), whereas that with mean summer temperature is unclear (Fig. 7c).

A positive correlation is generally expected between precipitation and runoff in glacier-free catchments. Furthermore, the mean summer temperature is expected to have a negative correlation with runoff through evaporation. However, glaciers yield an opposite response. More GMW is generated as the temperature increases, whereas an increase in precipitation would suppress surface melting by changing the surface heat balance due to high-albedo snow. The relationships shown in Fig. 7 support these opposite processes in glacierized and glacier-free catchments. Unlike the above explanation, the runoff response to precipitation seems unclear in glacier-affected catchments, except for the largest catchment. This unclear contribution of the glacier response to precipitation might reflect the fact that in a sufficiently warm environment, most of the precipitation falls as rain, which is not expected to suppress melting. This interpretation is supported by the results of a previous study of four Mongolian glaciers, whereby the correlations between mean summer temperature and glacier mass balance were very high (–0.87 to –0.96), whereas those between annual precipitation and glacier mass balance were moderate (0.54 to 0.78) (Khalzan et al., 2022). Of note, these correlations are with regard to glacier mass balance, such that the signs of the correlations are the opposite to those with GMW. The relationship between the correlation coefficient and GMW contribution is rather unclear among the observational data (Fig. 7c and d). This may be due to the temperature and precipitation observations being point data from a nearby station, such that their spatial variabilities in the catchment are not taken into account.

3.4.2. Extreme cases

We first calculated the runoff anomalies for the three most extreme years based on annual precipitation and mean summer temperature, which were normalized by dividing by the interannual variability (standard deviation) in each parameter. We also

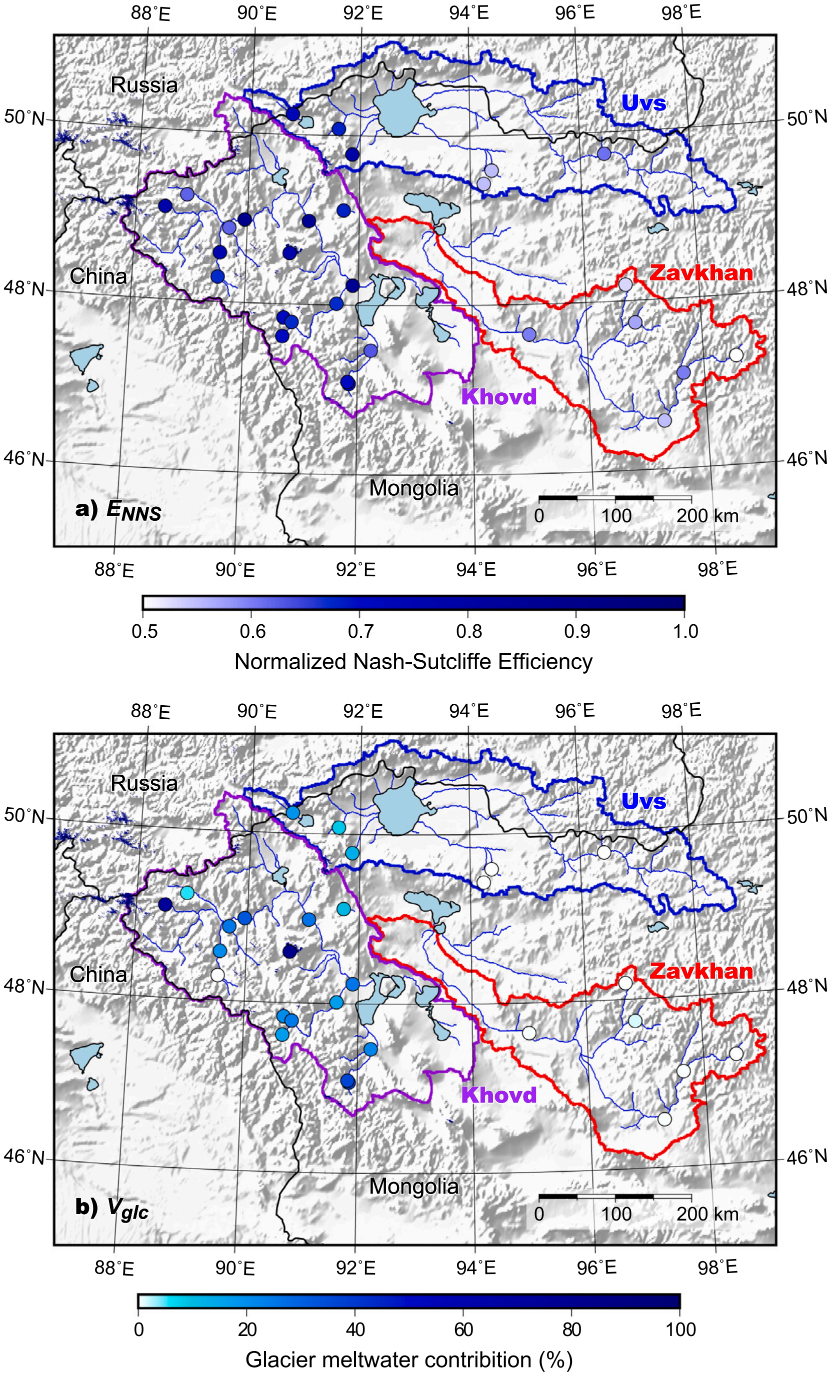

Fig. 5. (a) Normalized Nash–Sutcliffe efficiency (E_{NNS}) and (b) volume-based glacier meltwater contribution to river runoff (V_{glc}) at the 30 hydrological stations in western Mongolia.

calculated the corresponding annual runoff anomalies, and then quantitatively evaluated how fluctuations in the forcing variables affect river runoff (data listed in Table S3).

Fig. 8a and b show the runoff responses to precipitation extremes. Many catchments received about 1.7σ more precipitation during the three wettest years (Fig. 8a), whereas they received about 1.4σ less precipitation during the three driest years (Fig. 8b). This is probably because western Mongolia has an arid climate. The runoff anomalies are not significant in the glacier-free

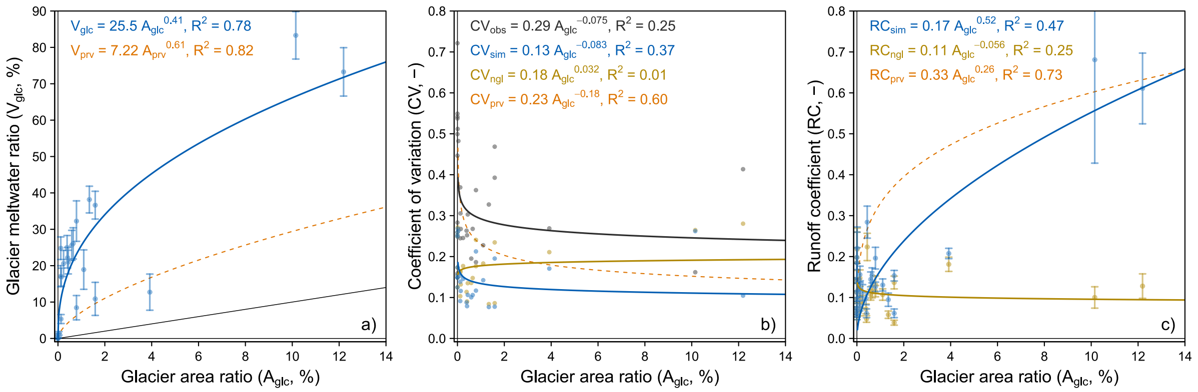

Fig. 6. Relationships of (a) volume-based glacier meltwater contribution (V_{glc}), (b) coefficient of variation of the annual runoff (CV), and (c) runoff coefficient (RC) against glacier area ratio (A_{glc}) and of the 30 catchments in western Mongolia. Subscripts glc, obs, sim, ngl, and prv denote glacier, observation, simulation, simulation with no-glacier configuration, and previous study by Zhang et al. (2016b), respectively. Data for the figure are listed in Table 3 and S1.

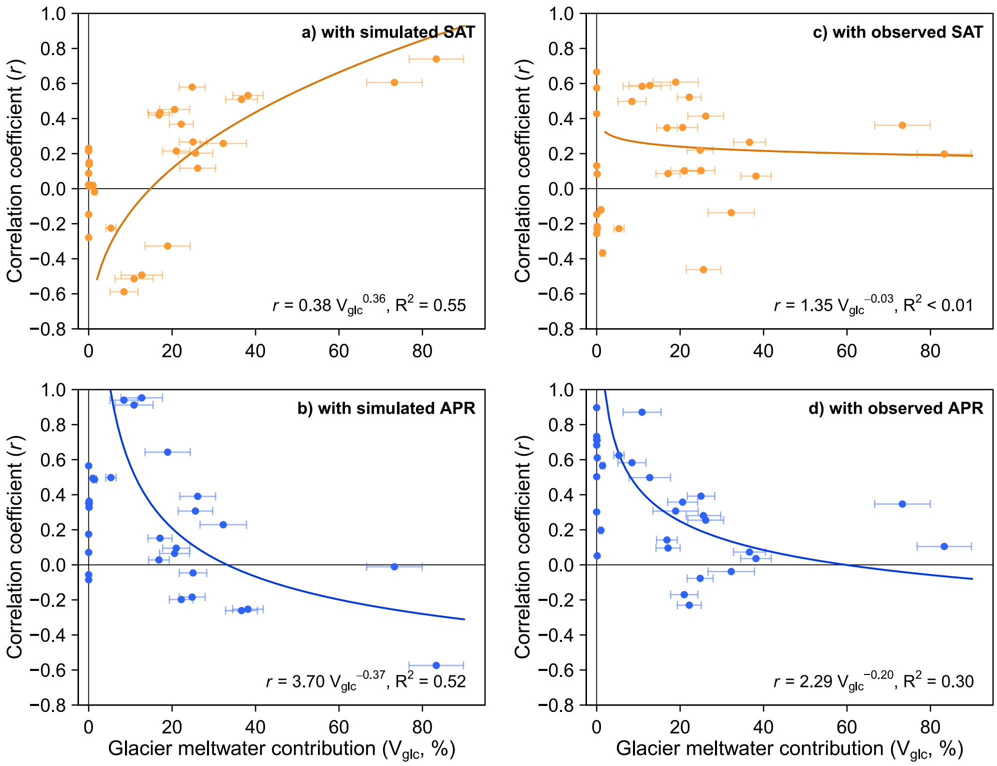

Fig. 7. Correlation coefficients of the annual runoff to (a) and (c) mean summer temperature (SAT), and (b) and (d) annual precipitation (APR) against the glacier meltwater contribution (V_{glc}) in terms of (a) and (b) simulation and ERA5, and (c) and (d) observational data at the 30 catchments in western Mongolia. For obtaining the fitting curves, data with V_{glc} < 2% were excluded. Values are listed in Table S2.

catchments. However, with increasing GMW contribution, the runoff anomaly tends to respond oppositely to the precipitation anomalies for both wet and dry extremes.

Fig. 8c and d show the effects of the temperature extremes. Under the warming situation (e.g. Cai et al., 2024), the mean summer temperature was 1.7σ colder during the three coldest summers (Fig. 8c) and 1.4σ warmer during the three warmest summers (Fig. 8d). The runoff responses are equivocal in the glacier-free catchments, as in the cases of extreme precipitation anomalies. Increasing

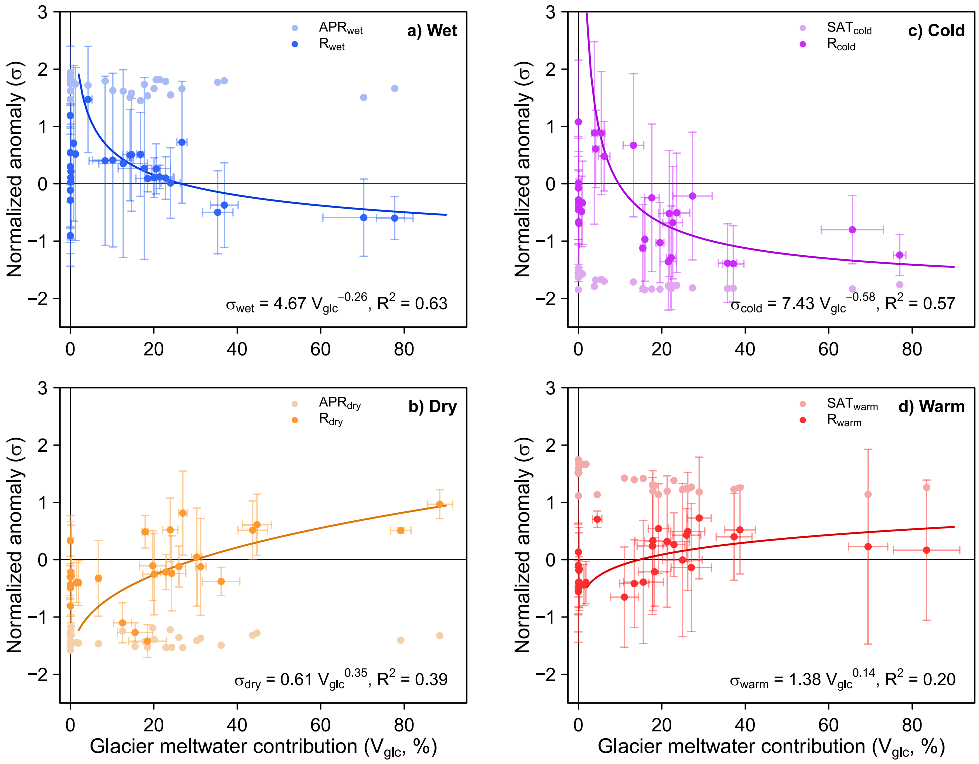

Fig. 8. Normalized anomaly of annual runoff (R), annual precipitation (APR), and mean summer temperature (SAT) in the extreme three years of (a) wet, (b) dry, (c) cold, and (d) warm for the 30 catchments in western Mongolia. For obtaining the fitting curves, data with $V_{glc} < 2\%$ were excluded. Values are listed in Table S3.

GMW contribution leads to a shift in the runoff anomaly during a cold anomaly from positive to negative (Fig. 8c), while it is unclear for the warm extremes (Fig. 8d).

4. Discussion

In glacier affected catchments, the GMW increases from May and contributes to sustain the river runoff from July to August (Fig. 4). This has been pointed out by Pan et al. (2019) though no quantitative evaluation was given. Considering the decrease in seasonal snow as a result of global warming, which is not considered in the simulation, it is expected that the peak runoff would decrease and the peak timing would appear earlier in the coming decades.

The estimated contribution of GMW to river runoff at Khovd Ulgii station (KhU) was 32.25% ± 5.56% in this study, which is much higher than the estimate of 8%–18% by the only previous study that evaluated the contribution of GMW to river runoff in western Mongolia (Pan et al., 2019). Pan et al. (2019) assumed a mass-balance gradient of 5.0 m water equivalent (w.e.) km^{-1}, whereas (Khalzan et al., 2022) proposed a physically estimated gradient of 6.4 m w.e. km^{-1}. Furthermore, Khalzan et al. (2022) noted and incorporated the high precipitation gradient with increasing elevation (40% km^{-1}), which was not considered by Pan et al. (2019).

For all panels of Fig. 6, power functional fitting curves reported in a previous study for glacierized catchments in Tien Shan are depicted (Zhang et al., 2016b). This study was selected for comparison because the Tien Shan region is geographically close to, and has a similar climate to, western Mongolia. In addition, Zhang et al. (2016b) simulated multiple catchments, making it suitable for comparing the characteristics of glacier meltwater contributions. The fitting curves suggest that the GMW contribution in western Mongolia is much greater than that calculated for the 24 catchments in Tien Shan (Fig. 6a). The coefficients of determination (R^2) for the coefficient of variations (CV_{obs} and CV_{sim}) are worse than that of Zhang et al. (2016b) (Fig. 6b), probably because Zhang et al. (2016b) calibrated their runoff parameters to fit the observed runoff. The runoff coefficient of this study (RC_{sim}) is less than that of Zhang et al. (2016b) (Fig. 6c), probably due to more arid environment in western Mongolia than that in Tien Shan.

The precipitation parameter is determined as a single value at each station (Fig. 3) and then a spatially fixed value. It means that the simulated interannual variabilities in runoff in glacier-free catchment are basically due to the interannual variability in ERA5 precipitation. The power functional fitting curve for CV (Fig. 6b) suggests that glaciers would contribute to suppress the interannual variability of river runoff through supplying more meltwater during the dry condition and vice versa. Similarly, the responses of runoff to precipitation and temperature extremes are explainable by those of glaciers; more meltwater in arid and warmer conditions and vice versa (Fig. 8). These analyses suggest that the presence of glaciers could mitigate the deficit in river runoff by supplying meltwater during drought conditions and thus suppress the interannual variability of river runoff (e.g. Zhang et al., 2016b; Pritchard, 2019).

The temporal changes in runoff show that the simulation does not well reproduce the long-term trend and intermittent large runoff events (Figures S3 and S4), probably because the ERA5 precipitation would not have good representativeness in this region for both long-term trend and events. The continuous shrinking glaciers could also affect the trend (Pan et al., 2019). However, the uncertainty in the GMW estimate is much greater than the glacier area change. In our simulations, accumulation, seasonal snowmelt, and the influence of permafrost on basal flow, which are not calibrated to the studied catchments, may explain the poor reproducibility of runoff in the glacier-free catchments.

5. Conclusions

This study is the first to undertake modeling of glacier-fed rivers in Mongolia using physically based models. We used the temperature and precipitation data from 28 meteorological stations across western Mongolia to calibrate the ERA5 reanalysis data and the runoff data from 30 hydrological stations to validate the simulated runoffs. There was a high reproducibility of the simulated runoffs in the Khovd River basin, which holds many glaciers, compared with the simulated runoffs in the Uvs Lake and Zavkhan River basins, where fewer glaciers are present. We consider the lack of permafrost-related hydrology in the models as one of the causes of the poorer reproducibility in the latter two basins. The volume-based glacier meltwater contributions were significantly larger than the glacier-area-based contributions, which suggests additional water supply from the shrinking glaciers and greater precipitation at higher elevations. Correlation analyses regarding the effects of air temperature and precipitation on river runoff were also conducted for the glacierized and glacier-free basins. Warming contributed to increased runoff in glacier-fed basins, and reduced runoff in glacier-free basins. Conversely, drought contributed to reduced runoff in glacier-free basins, whereas it could potentially increase glacier meltwater and consequently compensate for the decreased runoff in glacierized basins.

The results show that glaciers can modulate the response of river flow to climate change. These results provide a scientific basis for implementing integrated water resources management, including mitigation and adaptation plans for water resources, and gaining important insights into the hydrological dynamics of the region. Furthermore, the presented simulation scheme can be employed to evaluate changes in river runoff for future climate-change scenarios. This study highlights the need to further improve existing land-surface process and runoff models, as well as expand the network of meteorological, hydrological, and glacier observations, to better guide water resources management in a warming climate. On the other hand, it should be noted that the utilization of three distinct numerical models in this study introduced inherent limitations in computational efficiency, predictive accuracy, and comprehensive system-level analysis. To unveil critical synergistic effects between subsystems, further investigation for employing an integrated modeling framework is needed.

CRediT authorship contribution statement

Purevdagva Khalzan: Writing – original draft, Validation, Investigation, Formal analysis, Data curation. **Sanjar Sadyrov:** Writing – review & editing, Methodology. **Akiko Sakai:** Writing – review & editing, Project administration, Investigation, Funding acquisition, Conceptualization. **Kenji Tanaka:** Writing – review & editing, Methodology. **Koji Fujita:** Writing – original draft, Visualization, Methodology, Investigation, Funding acquisition, Formal analysis, Conceptualization.

Declaration of competing interest

The authors declare that they have no known competing financial interests or personal relationships that could have appeared to influence the work reported in this paper.

Acknowledgments

The authors would thank anonymous reviewers for their valuable inputs and reviews. This study is supported by JSPS, Japan-KAKENHI (JP20H00196 and JP25H00507) and the Transnational Doctoral Program for Leading Professionals in Asian Countries in Nagoya University, Japan.

Appendix A. Supplementary data

Supplementary material related to this article can be found online at https://doi.org/10.1016/j.ejrh.2025.102375.

Data availability

Monthly meteorological and hydrological observational data are available at https://doi.org/10.5281/zenodo.14729735 (Khalzan and Fujita, 2025). ERA5 reanalysis data are obtained from the Copernicus Climate Data Store (https://cds.climate.copernicus.eu/, last access: 8 May 2025). GTOPO30 data is obtained from the Earth Resources Observation and Science (EROS) Center (https://doi.org/10.5066/F7DF6PQS, last access: 8 May 2025).

References

Antokhina, O.Y., Latysheva, I.V., Mordvinov, V.I., 2019. A cases study of Mongolian cyclogenesis during the July 2018 blocking events. Geogr. Environ. Sustain. 12 (3), 66–78. https://doi.org/10.24057/2071-9388-2019-14.

Bantcev, D.V., Ganyushkin, D.A., Chistyakov, K.V., Volkov, I.V., Ekaykin, A.A., Veres, A.N., Tokarev, I.V., Shtykova, N.B., Andreeva, T.A., 2019. The components of the glacial runoff of the Tsambagarav massif from stable water isotope data. Geosciences 9 (7), 297. https://doi.org/10.3390/geosciences9070297.

Batimaa, P., Myagmarjav, B., Batnasan, N., Jadambaa, N., Khishigsuren, P., 2011. Urban water vulnerability to climate change in Mongolia.

Batsukh, N., Dorjsuren, D., Batsaikhan, G., 2008. The water resources, use and conservation in Mongolia (First national report). In: Report Prepared for the National Water Committee of Mongolia. Mongolian Ministry of Nature and Environment, Ulaanbaatar.

Cai, Q., Chen, W., Chen, S., Xie, S.-P., Piao, J., Ma, T., Lan, X., 2024. Recent pronounced warming on the Mongolian Plateau boosted by internal climate variability. Nat. Geosci. 17 (3), 181–188. https://doi.org/10.1038/s41561-024-01377-6.

Champeaux, J.L., Masson, V., Chauvin, F., 2005. ECOCLIMAP: A global database of land surface parameters at 1 km resolution. Meteorol. Appl. 12 (1), 29–32. https://doi.org/10.1017/S1350482705001519.

Cosby, B., Hornberger, G., Clapp, R., Ginn, T., 1984. A statistical exploration of the relationships of soil moisture characteristics to the physical properties of soils. Water Resour. Res. 20 (6), 682–690. https://doi.org/10.1017/S1350482705001519.

Dashdeleg, N., Evilkhaan, R., Khishigsuren, P., 1983. Modern glaciers in the Altai Mountains. Proc. Inst. Meteorol. Hydrol. 8, 121–126.

Davaa, G., 2010. Climate change impact on water resources in Mongolia. pp. 30–36.

Deardorff, J.W., 1977. A parameterization of ground-surface moisture content for use in atmospheric prediction models. J. Appl. Meteorol. 16 (11), 1182–1185.

Dgebuadze, Y., Batnasan, N., Berdovskaya, G., Verzilin, N., Devyatkin, E., Dorofeyuk, N., Dulmaa, A., Egorov, A., Kalmykova, N., Korneva, L., Kosolapova, N., Krylov, A., Kulikovsky, M., Liiva, A., Luvsandorzh, N., Martinson, G., Mensaikhan, B., Neustrueva, I., Nikolaeva, T., Petukhov, V., Ponomarenko, A., Przhiboro, A., Prokin, A., Rasskazov, A., Sanchir, G., Sevastyanov, D., Skvortsov, V., Hand, Y., Tsarenko, P., Tsugar, S., Tseresodnom, J., Tsetsegmaa, D., Chebotarev, E., Shuvalov, V., 2014. Lynmology and paleolymnology of Mongolia.

Fujita, K., Ageta, Y., 2000. Effect of summer accumulation on glacier mass balance on the Tibetan Plateau revealed by mass-balance model. J. Glaciol. 46 (153), 244–252. https://doi.org/10.3189/172756500781832945.

Fujita, K., Ohta, T., Ageta, Y., 2007. Characteristics and climatic sensitivities of runoff from a cold-type glacier on the Tibetan Plateau. Hydrol. Process. 21 (21), 2882–2891. https://doi.org/10.1002/hyp.6505.

Fujita, K., Sakai, A., 2014. Modelling runoff from a Himalayan debris-covered glacier. Hydrol. Earth Syst. Sci. 18 (7), 2679–2694. https://doi.org/10.5194/hess-18-2679-2014.

Garmaev, E.Z., Bolgov, M., Ayurzhanaev, A., Tsydypov, B., 2019. Water resources in Mongolia and their current state. Russ. Meteorol. Hydrol. 44 (10), 659–666. https://doi.org/10.3103/S1068373919100030.

Grunert, J., Lehmkuhl, F., Walther, M., 2000. Paleoclimatic evolution of the Uvs Nuur basin and adjacent areas (Western Mongolia). Quat. Int. 65–66, 171–192. https://doi.org/10.1016/S1040-6182(99)00043-9.

Hersbach, H., Bell, B., Berrisford, P., Hirahara, S., Horányi, A., Muñoz-Sabater, J., Nicolas, J., Peubey, C., Radu, R., Schepers, D., Simmons, A., Soci, C., Abdalla, S., Abellan, X., Balsamo, G., Bechtold, P., Biavati, G., Bidlot, J., Bonavita, M., De Chiara, G., Dahlgren, P., Dee, D., Diamantakis, M., Dragani, R., Flemming, J., Forbes, R., Fuentes, M., Geer, A., Haimberger, L., Healy, S., Hogan, R.J., Hólm, E., Janisková, M., Keeley, S., Laloyaux, P., Lopez, P., Lupu, C., Radnoti, G., de Rosnay, P., Rozum, I., Vamborg, F., Villaume, S., Thépaut, J.-N., 2020. The ERA5 global reanalysis. Q. J. R. Meteorol. Soc. 146 (730), 1999–2049. https://doi.org/10.1002/qj.3803.

Hugonnet, R., McNabb, R., Berthier, E., Menounos, B., Nuth, C., Girod, L., Farinotti, D., Huss, M., Dussaillant, I., Brun, F., Kääb, A., 2021. Accelerated global glacier mass loss in the early twenty-first century. Nature 592 (7856), 726–731. https://doi.org/10.1038/s41586-021-03436-z.

Kadota, T., Davaa, G., 2007. Recent glacier variations in Mongolia. Ann. Glaciol. 46, 185–188. https://doi.org/10.3189/172756407782871675.

Kadota, T., Davaa, G., Khalzan, P., Davaadorj, N., Ohata, T., 2011. Glaciological research in the Mongolian Altai, 2003–2009. Bull. Glaciol. Res. 29, 41–50. https://doi.org/10.5331/bgr.29.41.

Kamp, U., McManigal, K.G., Dashtseren, A., Walther, M., 2013. Documenting glacial changes between 1910, 1970, 1992 and 2010 in the Turgen Mountains, Mongolian Altai, using repeat photographs, topographic maps, and satellite imagery. Geogr. J. 179 (3), 248–263. https://doi.org/10.1111/j.1475-4959.2012.00486.x.

Kamp, U., Pan, C.G., 2015. Inventory of glaciers in Mongolia, derived from landsat imagery from 1989 to 2011. Geogr. Ann.: Ser. A, Phys. Geogr. 97 (4), 653–669. https://doi.org/10.1111/geoa.12105.

Khalzan, P., Fujita, K., 2025. Meteorological, hydrological, and glaciological data in western Mongolia. https://doi.org/10.5281/zenodo.14729735.

Khalzan, P., Sakai, A., Fujita, K., 2022. Mass balance of four Mongolian glaciers: In-situ measurements, long-term reconstruction and sensitivity analysis. Front. Earth Sci. 9, 785306. https://doi.org/10.3389/feart.2021.785306.

Konya, K., Kadota, T., Nakazawa, F., Davaa, G., Khalzan, P., Ohata, T., 2010. Surface mass balance of the Potanin Glacier in the Mongolian Altai Mountains and comparison with Russian Altai glaciers in 2005, 2008, and 2009. Bull. Glaciol. Res. 31, 9–18. https://doi.org/10.5331/bgr.31.9.

Kottek, M., Grieser, J., Beck, C., Rudolf, B., Rubel, F., 2006. World map of the Köppen-Geiger climate classification updated. Geogr. Environ. Sustain. 15 (3), 259–263. https://doi.org/10.1127/0941-2948/2006/0130.

Lehner, B., Grill, G., 2013. Global river hydrography and network routing: Baseline data and new approaches to study the world's large river systems. Hydrol. Process. 27 (15), 2171–2186. https://doi.org/10.1002/hyp.9740.

Loveland, T.R., Reed, B.C., Brown, J.F., Ohlen, D.O., Zhu, Z., Yang, L., Merchant, J.W., 2000. Development of a global land cover characteristics database and IGBP DISCover from 1 km AVHRR data. Int. J. Remote Sens. 21 (6–7), 1303–1330. https://doi.org/10.1080/014311600210191.

Mathevet, T., Michel, C., Andréassian, V., Perrin, C., 2006. A bounded version of the Nash-sutcliffe criterion for better model assessment on large sets of basins. IAHS Publ. 307, 211–219.

Minowa, M., Skvarca, P., Fujita, K., 2023. Climate and surface mass balance at Glaciar Perito Moreno, southern Patagonia. J. Clim. 36 (2), 625–641. https://doi.org/10.1175/JCLI-D-22-0294.1.

Motoya, K., Kondo, J., 1999. Estimating the seasonal variations of snow water equivalent, runoff and water temperature of a stream in a basin using the new bucket model. J. Jpn. Soc. Hydrol. Water Resour. 12 (5), 391–407. https://doi.org/10.3178/jjshwr.12.391.

Munkhbat, B., Gomboluudev, P., Erdenesukh, S., Sandelger, D., 2022. To estimate air temperature and precipitation of mongolia (1991–2020) for the high-resolution grid using ANUSPLIN statistical model. Geogr. Issues 22 (1), 92–102.

Nash, J.E., Sutcliffe, J.V., 1970. River flow forecasting through conceptual models part I – a discussion of principles. J. Hydrol. 10 (3), 282–290. https://doi.org/10.1016/0022-1694(70)90255-6.

Nuimura, T., Sakai, A., Taniguchi, K., Nagai, H., Lamsal, D., Tsutaki, S., Kozawa, A., Hoshina, Y., Takenaka, S., Omiya, S., Tsunematsu, K., Tshering, P., Fujita, K., 2015. The GAMDAM glacier inventory: A quality-controlled inventory of Asian glaciers. Cryosphere 9 (3), 849–864. https://doi.org/10.5194/tc-9-849-2015.

Ochir, A., Munkhjargal, M., Bat-Erdene, A., Tsetsgee, S., 2013. Zavkhan river and its catchment area delineation using satellite image. J. Water Resour. Prot. 5 (10), 38237. https://doi.org/10.4236/jwarp.2013.510095.

Orkhonselenge, A., Harbor, J.M., 2018. Impacts of modern glacier changes on surface water resources in western and northern Mongolia. J. Water Resour. Prot. 10 (6), 85579. https://doi.org/10.4236/jwarp.2018.106031.

Pan, C.G., Kamp, U., Munkhjargal, M., Halvorson, S.J., Dashtseren, A., Walther, M., 2019. An estimated contribution of glacier runoff to Mongolia's Upper Khovd River Basin in the Altai Mountains. Mt. Res. Dev. 39 (2), R12–R20. https://doi.org/10.1659/MRD-JOURNAL-D-18-00059.1.

Pan, C.G., Pope, A., Kamp, U., Dashtseren, A., Walther, M., Syromyatina, M.V., 2018. Glacier recession in the Altai Mountains of Mongolia in 1990–2016. Geogr. Ann.: Ser. A, Phys. Geogr. 100 (2), 185–203. https://doi.org/10.1080/04353676.2017.1407560.

Pritchard, H.D., 2019. Asia's shrinking glaciers protect large populations from drought stress. Nature 569 (7758), 649–654. https://doi.org/10.1038/s41586-019-1240-1.

Sadyrov, S., Tanaka, K., Satylkanov, R., Khujanazarov, T., Touge, Y., Fujita, K., 2024. Modelling runoff components and hydrological processes in glaciated catchments of the inner Tien-Shan, Kyrgyzstan. Front. Earth Sci. 11, 1306476. https://doi.org/10.3389/feart.2023.1306476.

Sakai, A., 2019. Brief communication: Updated GAMDAM glacier inventory over high-mountain Asia. Cryosphere 13 (7), 2043–2049. https://doi.org/10.5194/tc-13-2043-2019.

Sakai, A., Fujita, K., Nakawo, M., Yao, T., 2009. Simplification of heat balance calculation and its application to the glacier runoff from the July 1st Glacier in northwest China since the 1930s. Hydrol. Process. 23 (4), 585–596. https://doi.org/10.1002/hyp.7187.

Sakai, A., Fujita, K., Narama, C., Kubota, J., Nakawo, M., Yao, T., 2010. Reconstructions of annual discharge and equilibrium line altitude of glaciers at Qilian Shan, northwest China, from 1978 to 2002. Hydrol. Process. 24 (19), 2798–2806. https://doi.org/10.1002/hyp.7700.

Sato, T., Tsujimura, M., Yamanaka, T., Iwasaki, H., Sugimoto, A., Sugita, M., Kimura, F., Davaa, G., Oyunbaatar, D., 2007. Water sources in semiarid northeast Asia as revealed by field observations and isotope transport model. J. Geophys. Res.: Atmospheres 112 (D17), D17112. https://doi.org/10.1029/2006JD008321.

Sayama, T., Ozawa, G., Kawakami, T., Nabesaka, S., Fukami, K., 2012. Rainfall–runoff–inundation analysis of the 2010 Pakistan flood in the Kabul River basin. Hydrol. Sci. J. 57 (2), 298–312. https://doi.org/10.1080/02626667.2011.644245.

Sellers, P., Mintz, Y., Sud, Y., Dalcher, A., 1986. A simple biosphere model (SiB) for use within general circulation models. J. Atmos. Sci. 43 (6), 505–531. https://doi.org/10.1175/1520-0469(1986)043.

Sellers, P., Randall, D., Collatz, G., Berry, J., Field, C., Dazlich, D., Zhang, C., Collelo, G., Bounoua, L., 1996. A revised land surface parameterization (SiB2) for atmospheric GCMs. Part I: Model formulation. J. Clim. 9 (4), 676–705. https://doi.org/10.1175/1520-0442(1996)009.

Syromyatina, M., Kurochkin, Y., Bliakharskii, D., Chistyakov, K., 2015. Current dynamics of glaciers in the Tavan Bogd Mountains (Northwest Mongolia). Environ. Earth Sci. 74, 1905–1914. https://doi.org/10.1007/s12665-015-4606-1.

Tachikawa, T., Hato, M., Kaku, M., Iwasaki, A., 2011. Characteristics of ASTER GDEM version 2. In: In 2011 IEEE International Geoscience and Remote Sensing Symposium. IEEE, pp. 3657–3660. https://doi.org/10.1109/IGARSS.2011.6050017.

Tanaka, K., 2005. Development of the new land surface scheme SiBUC commonly applicable to basin water management and numerical weather prediction model (Ph.D. thesis). Kyoto University, Kyoto, Japan.

Zhang, Y., Enomoto, H., Ohata, T., Kitabata, H., Kadota, T., Hirabayashi, Y., 2017. Glacier mass balance and its potential impacts in the Altai Mountains over the period 1990–2011. J. Hydrol. 553, 662–677. https://doi.org/10.1016/j.jhydrol.2017.08.026.

Zhang, Y., Hirabayashi, Y., Fujita, K., Liu, S., Liu, Q., 2016a. Heterogeneity in supraglacial debris thickness and its role in glacier mass changes of the Mount Gongga. Sci. China Earth Sci. 59, 170–184. https://doi.org/10.1007/s11430-015-5118-2.

Zhang, Y., Luo, Y., Sun, L., Liu, S., Chen, X., Wang, X., 2016b. Using glacier area ratio to quantify effects of melt water on runoff. J. Hydrol. 538, 269–277. https://doi.org/10.1016/j.jhydrol.2016.04.026.

Supporting Information for "Glacier meltwater contribution to river runoff in Western Mongolia"

Purevdagva Khalzan[a,b], Sanjar Sadyrov[c,d], Akiko Sakai[b], Kenji Tanaka[d], Koji Fujita[b]

[a] *Information and Research Institute of Meteorology Hydrology and Environment, Ulaanbaatar, 15160, Mongolia*
[b] *Graduate School of Environmental Studies, Nagoya University, Chikusa-ku, Nagoya, 464-8601, Japan*
[c] *Mountain Societies Research Institute, University of Central Asia, Bishkek, 720001, Kyrgyzstan*
[d] *Disaster Prevention Research Institute, Kyoto University, Uji, 611-0011, Japan*

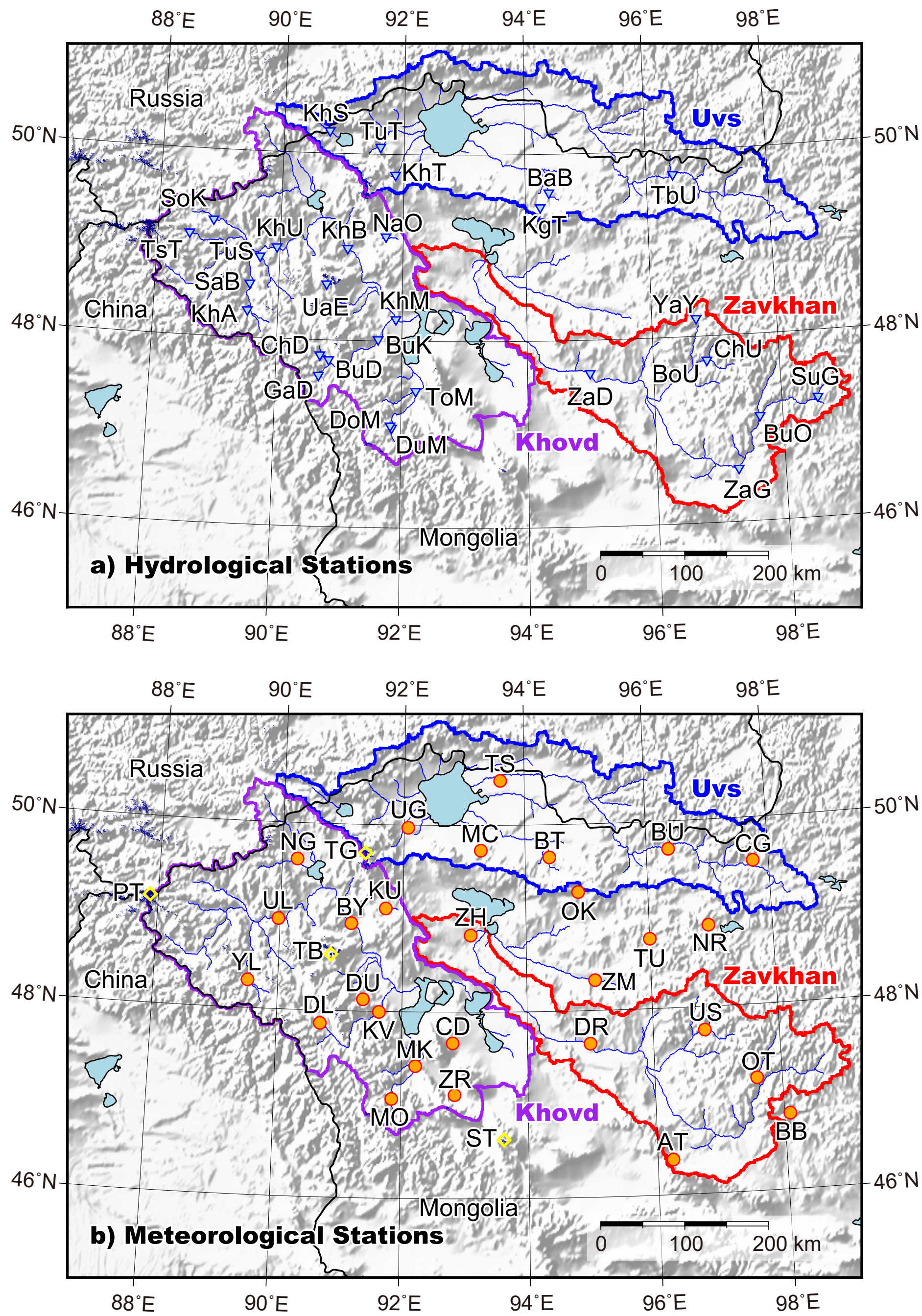

Figure S1: a) Hydrological stations, and b) meteorological stations and glaciers in western Mongolia. Details of the stations including abbreviation are listed in Tables 1 and 2.

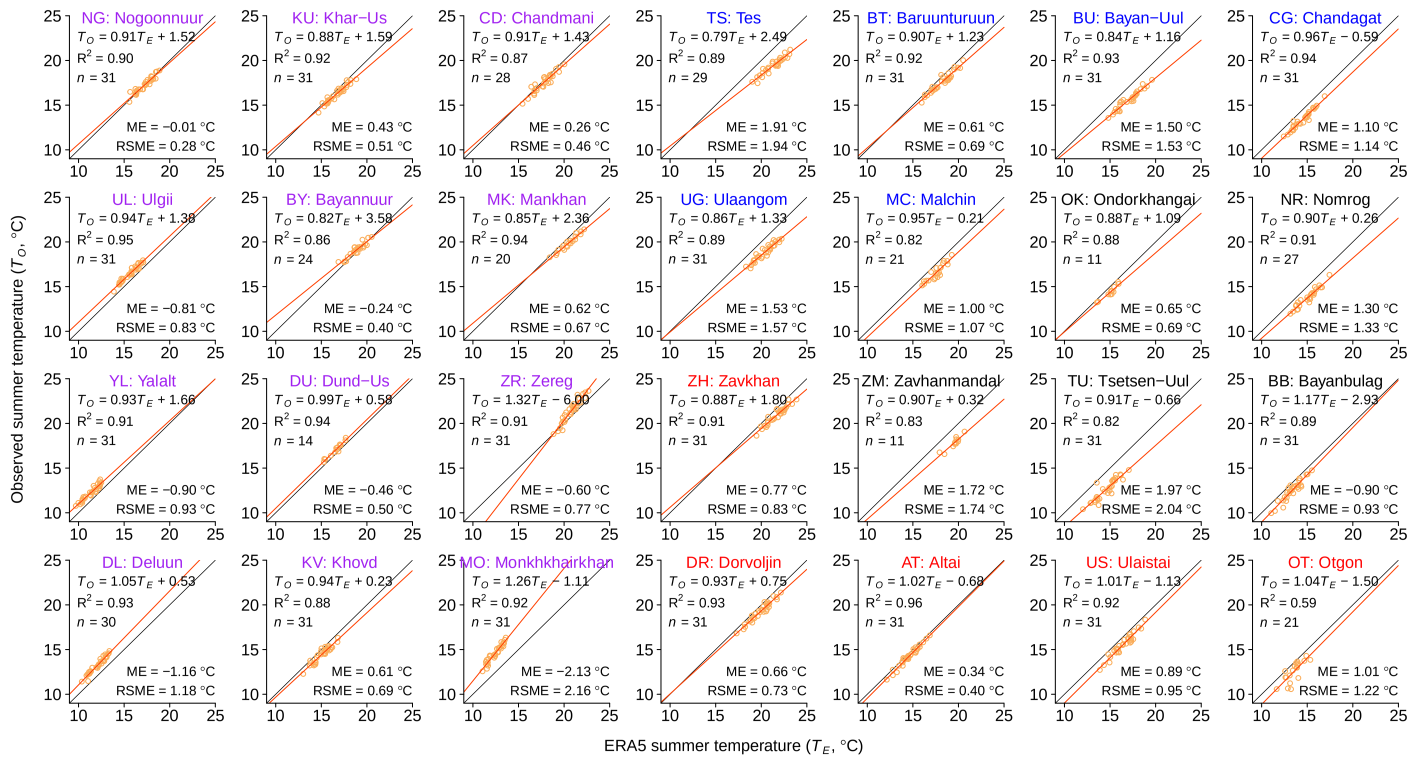

Figure S2: Comparison of mean summer temperatures of ERA5 (T_E, horizontal axes) and observation (T_O, vertical axes) at the 28 meteorological stations in western Mongolia. Text colors of the station correspond to the large basins (Figure 1).

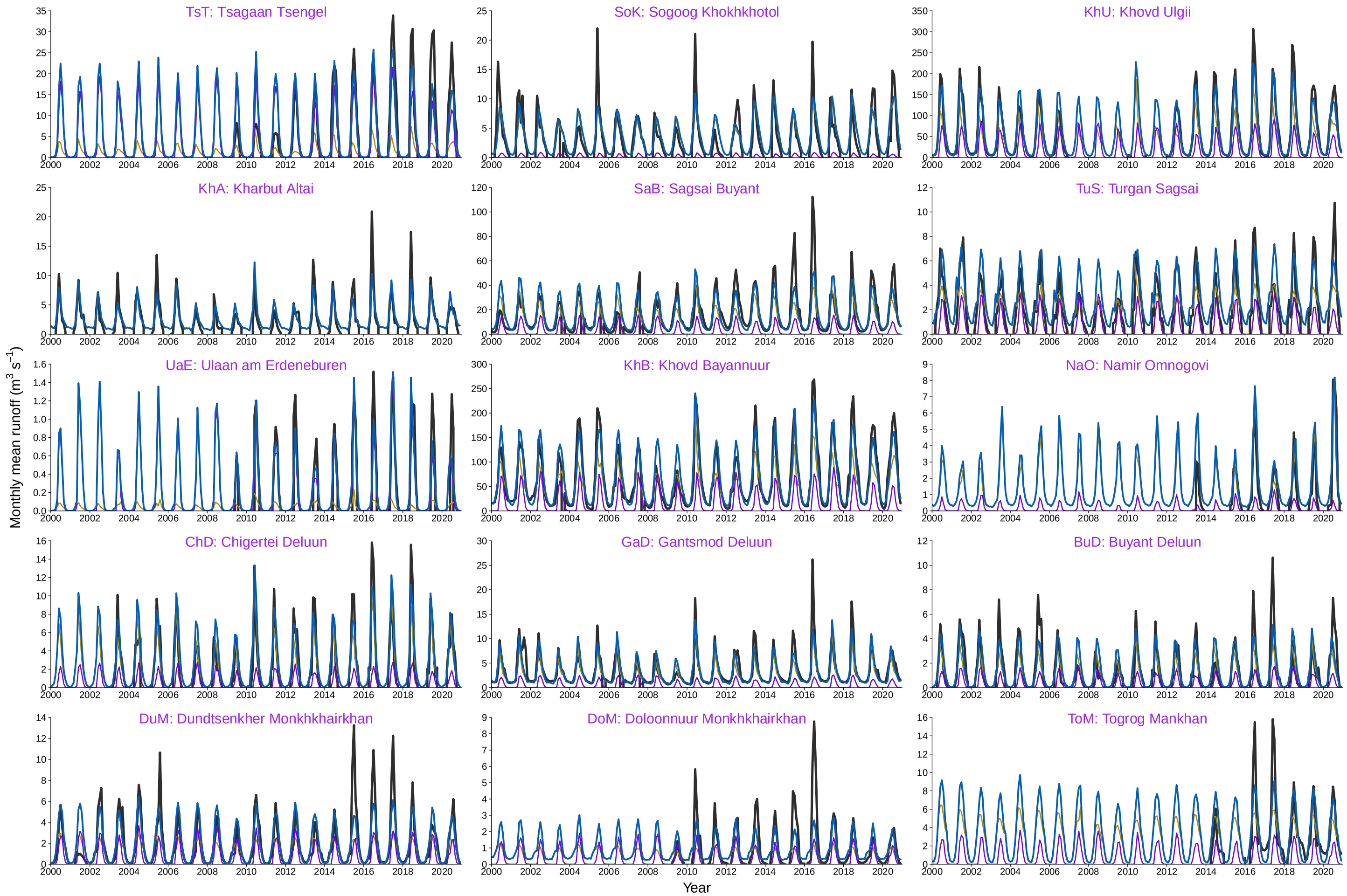

Figure S3: Observed (black) and simulated (blue) monthly mean runoff at the 30 hydrological stations in western Mongolia. Purple and brown lines denote glacier meltwater and runoff without glacier configuration, respectively. Text colors correspond to those for the large basins (Figure 1).

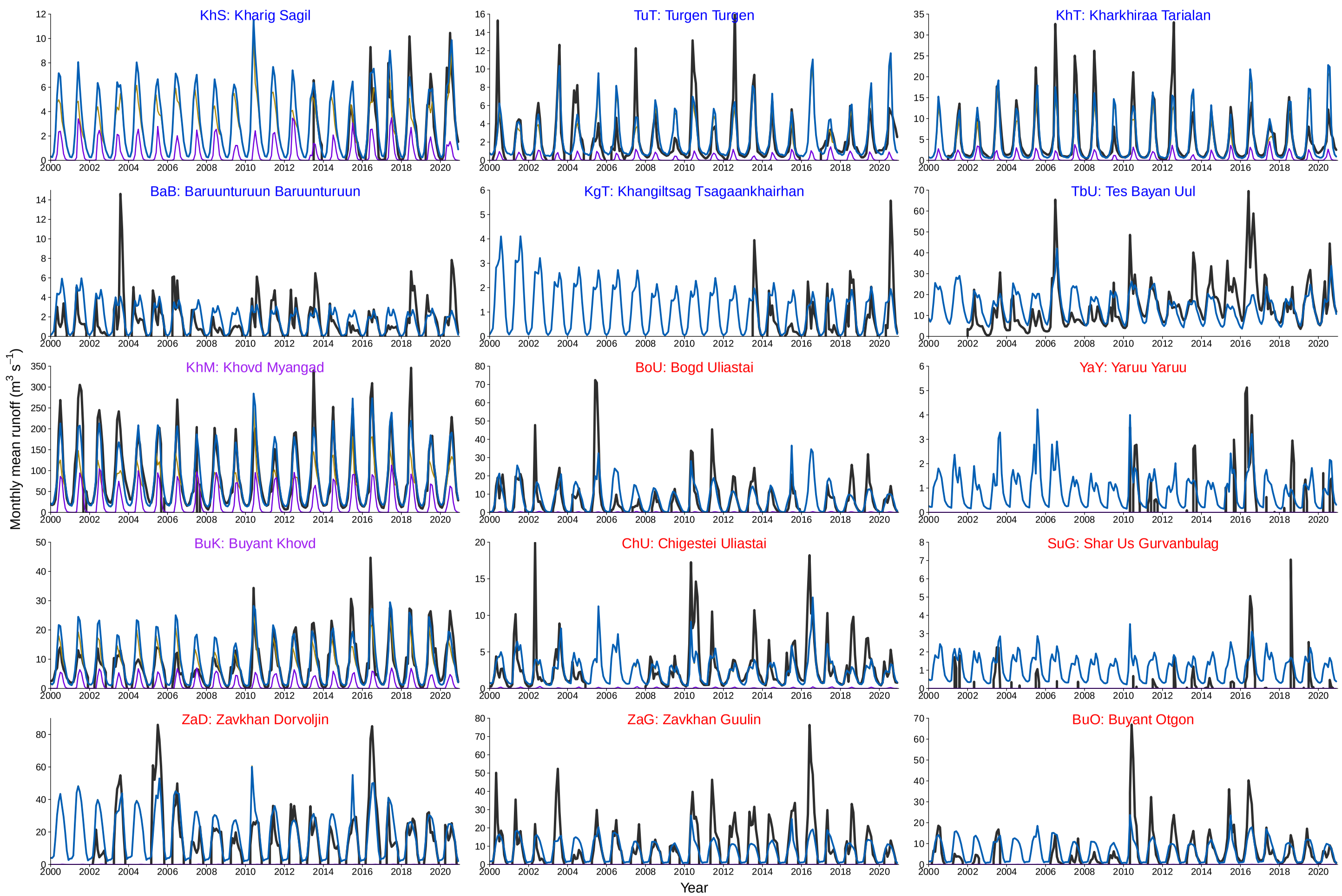

Figure S4: Figure S3 continued.

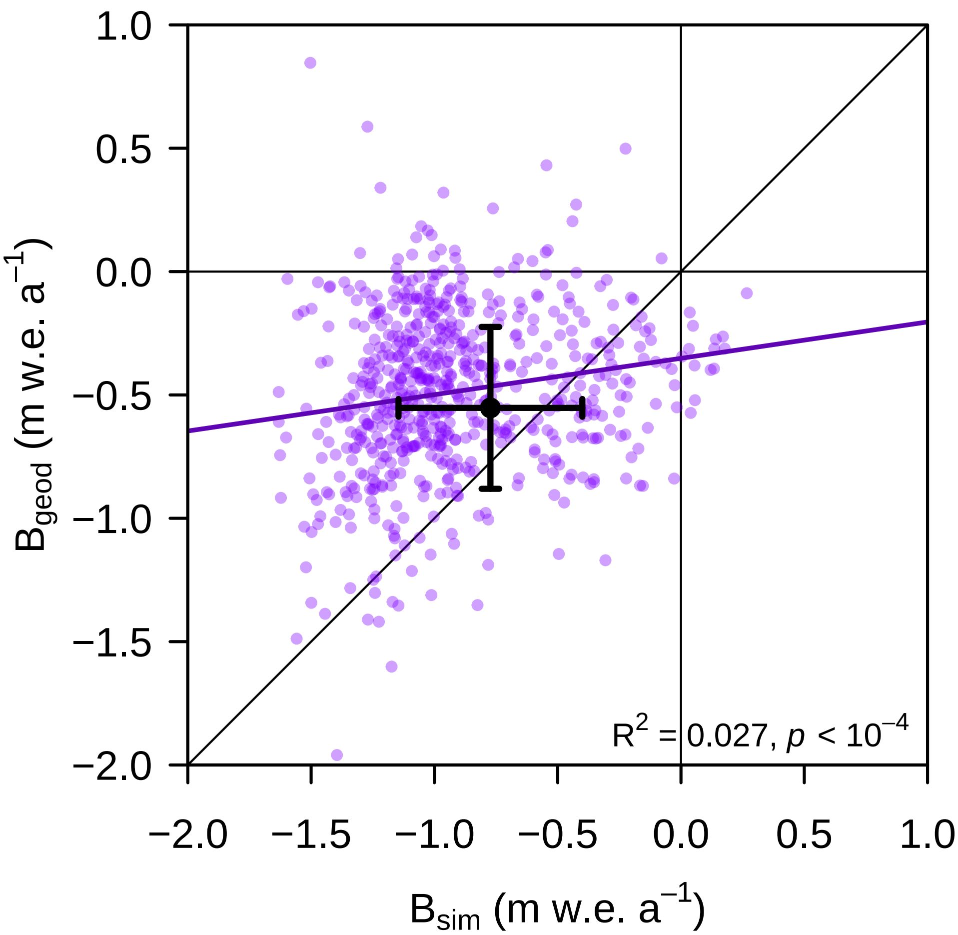

Figure S5: Simulated (B_{sim}) and remotely sensed geodetic (B_{geod}) mass balance of 652 glaciers in western Mongolia averaged for the period 2000-2020. B_{geod} are adopted from Hugonnet et al. (2021). Purple line denotes a linear regression ($R^2 = 0.027$, $p < 10^{-4}$). Black circle with error cross denotes the area-weighted mean and their standard deviation (1σ) for all glaciers.

Table S1: Coefficients of variation (CV) and Runoff coefficients (RC) for simulated and observed river runoffs in western Mongolia. Subscriptions obs, dis, and ngl denote observation, simulation and simulation with no-glacier configuration, respectively.

Station code	CV_{obs}	CV_{sim}	CV_{ngl}	RC_{sim}	RC_{ngl}
TsT	0.41	0.10	0.28	0.61±0.09	0.13±0.03
SoK	0.31	0.15	0.16	0.16±0.02	0.15±0.02
KhA	0.28	0.15	0.15	0.06±0.01	0.06±0.01
SaB	0.30	0.11	0.14	0.28±0.04	0.22±0.03
TuS	0.26	0.09	0.11	0.10±0.02	0.07±0.01
KhU	0.19	0.12	0.18	0.20±0.03	0.13±0.02
KhB	0.27	0.11	0.15	0.15±0.02	0.11±0.01
UaE	0.16	0.26	0.26	0.68±0.25	0.10±0.03
NaO	0.39	0.20	0.23	0.15±0.01	0.14±0.02
ChD	0.25	0.15	0.18	0.11±0.02	0.09±0.02
GaD	0.24	0.14	0.16	0.08±0.01	0.07±0.01
BuD	0.37	0.09	0.10	0.12±0.02	0.09±0.01
BuK	0.27	0.12	0.13	0.12±0.02	0.10±0.02
KhM	0.20	0.10	0.14	0.14±0.02	0.11±0.01
DuM	0.33	0.08	0.08	0.09±0.02	0.06±0.01
DoM	0.47	0.08	0.09	0.06±0.01	0.04±0.01
ToM	0.25	0.08	0.09	0.06±0.01	0.05±0.01
KhS	0.23	0.14	0.18	0.13±0.01	0.11±0.01
TuT	0.36	0.21	0.24	0.13±0.01	0.12±0.01
KhT	0.27	0.17	0.21	0.21±0.01	0.18±0.02
KgT	0.55	0.25	0.25	0.20±0.06	0.20±0.06
BaB	0.54	0.26	0.26	0.14±0.04	0.14±0.04
TbU	0.45	0.16	0.16	0.10±0.02	0.10±0.02
YaY	0.16	0.25	0.25	0.18±0.04	0.18±0.04
ChU	0.48	0.26	0.27	0.12±0.03	0.12±0.03
BoU	0.51	0.27	0.27	0.22±0.05	0.22±0.05
SuG	0.83	0.12	0.12	0.11±0.02	0.11±0.02
BuO	0.72	0.15	0.15	0.07±0.01	0.07±0.01
ZaG	0.50	0.15	0.15	0.06±0.01	0.06±0.01
ZaD	0.54	0.17	0.17	0.06±0.01	0.06±0.01

Table S2: Correlation coefficients of simulated and observed river runoffs to mean summer temperature (SAT) and annual precipitation (APR) in western Mongolia. Meteorological station code denotes the station whose data are used to obtain the observed correlation coefficients.

Station code	Simulated r_{SAT}	Simulated r_{APR}	Observed r_{SAT}	Observed r_{APR}	Meteorological station code
TsT	0.606	–0.011	0.362	0.347	UL
SoK	–0.225	0.498	–0.228	0.625	UL
KhA	0.088	0.175	0.428	0.503	YL
SaB	0.215	0.095	0.102	–0.170	YL
TuS	0.267	–0.046	0.103	0.392	YL
KhU	0.258	0.229	–0.137	–0.038	UL
KhB	0.117	0.391	0.414	0.255	BY
UaE	0.748	–0.574	0.198	0.105	BY
NaO	–0.514	0.912	0.584	0.871	KU
ChD	0.452	0.065	0.349	0.358	DL
GaD	0.434	0.152	0.086	0.096	DL
BuD	0.580	–0.184	0.220	–0.077	DL
BuK	0.421	0.028	0.347	0.142	KV
KhM	0.203	0.307	–0.462	0.281	KV
DuM	0.532	–0.253	0.072	0.036	MK
DoM	0.509	–0.261	0.265	0.073	MK
ToM	0.368	–0.198	0.522	–0.230	MK
KhS	–0.327	0.643	0.608	0.307	UG
TuT	–0.588	0.940	0.498	0.583	UG
KhT	–0.493	0.953	0.589	0.498	UG
KgT	0.230	–0.085	0.575	0.897	BT
BaB	0.215	0.071	0.666	0.733	BT
TbU	–0.147	–0.056	–0.147	0.302	BU
YaY	–0.279	0.565	–0.256	0.714	US
ChU	–0.018	0.487	–0.367	0.566	US
BoU	0.019	0.493	–0.121	0.197	US
SuG	0.022	0.353	0.131	0.683	OT
BuO	0.150	0.350	0.084	0.611	OT
ZaG	0.139	0.328	–0.232	0.711	AT
ZaD	0.014	0.363	–0.216	0.052	DR

Table S3: Normalized anomalies of runoff (R) with those of annual precipitation (APR) and mean summer temperature (SAT) at the 30 catchments in western Mongolia. For each case, the three extreme years are selected. All variables are normalized with their standard deviations (Tables 2 and 3).

Station code	R_{dry}	APR_{dry}	R_{wet}	APR_{wet}	R_{cold}	SAT_{cold}	R_{warm}	SAT_{warm}
TsT	0.51±0.04	–1.40±0.62	–0.59±0.67	1.51±0.31	–0.80±0.60	–1.83±0.40	0.23±1.70	1.14±0.04
SoK	–0.35±0.66	–1.47±0.32	1.47±0.93	1.72±0.44	0.89±1.59	–1.79±0.35	0.71±0.14	1.14±0.08
KhA	–0.30±0.36	–1.58±0.10	0.54±0.86	1.47±0.17	0.01±1.08	–1.85±0.16	0.13±1.39	1.11±0.10
SaB	–0.22±0.31	–1.53±0.17	0.09±0.23	1.53±0.31	–0.25±1.29	–1.84±0.14	0.54±0.78	1.14±0.11
TuS	–0.12±0.36	–1.36±0.22	0.12±0.21	1.82±0.11	–0.52±1.10	–1.80±0.13	–0.01±1.34	1.22±0.13
KhU	–0.38±0.25	–1.49±0.20	0.72±1.06	1.66±0.24	–0.21±1.12	–1.82±0.18	0.73±1.06	1.18±0.08
KhB	–0.12±0.85	–1.37±0.28	0.26±0.44	1.82±0.30	–0.51±1.04	–1.77±0.22	0.43±0.46	1.25±0.06
UaE	0.97±0.25	–1.33±0.44	–0.60±0.37	1.66±0.30	–1.24±0.36	–1.76±0.22	0.17±1.22	1.26±0.24
NaO	–1.27±0.17	–1.51±0.45	0.41±1.52	1.63±0.34	0.88±1.07	–1.67±0.21	–0.42±0.76	1.40±0.32
ChD	–0.24±0.66	–1.53±0.21	0.51±0.73	1.45±0.08	–1.03±0.70	–1.84±0.18	0.32±1.15	1.20±0.11
GaD	–0.25±0.71	–1.39±0.02	0.50±0.80	1.51±0.18	–0.97±0.73	–1.85±0.17	0.33±1.22	1.20±0.10
BuD	0.81±0.73	–1.54±0.37	0.01±0.61	1.55±0.15	–1.29±0.91	–1.83±0.18	0.49±1.03	1.23±0.12
BuK	0.49±0.28	–1.43±0.21	0.51±0.99	1.58±0.36	–1.12±0.76	–1.83±0.09	0.24±1.20	1.31±0.14
KhM	0.05±0.86	–1.41±0.24	0.11±0.35	1.66±0.21	–0.68±0.98	–1.78±0.14	–0.14±1.12	1.27±0.16
DuM	0.61±0.53	–1.28±0.12	–0.37±0.74	1.80±0.46	–1.40±0.66	–1.82±0.09	0.52±0.77	1.25±0.15
DoM	0.52±0.51	–1.32±0.10	–0.50±0.72	1.77±0.41	–1.39±0.69	–1.83±0.08	0.40±0.76	1.23±0.13
ToM	0.52±0.56	–1.22±0.12	0.10±0.37	1.79±0.80	–1.36±0.84	–1.78±0.17	0.26±0.56	1.38±0.19
KhS	–0.11±0.61	–1.19±0.05	0.27±1.59	1.73±0.68	0.67±1.25	–1.71±0.37	–0.21±0.60	1.29±0.18
TuT	–1.10±0.35	–1.25±0.17	0.40±1.48	1.79±0.41	0.61±0.68	–1.68±0.29	–0.65±0.87	1.42±0.23
KhT	–1.42±0.28	–1.53±0.27	0.35±1.64	1.62±0.27	0.48±0.61	–1.70±0.29	–0.39±1.07	1.42±0.27
KgT	–0.49±0.30	–1.52±0.24	–0.91±0.12	1.62±0.42	–0.36±0.61	–1.63±0.10	–0.49±0.47	1.51±0.37
BaB	–0.44±0.37	–1.51±0.33	–0.11±1.11	1.74±0.22	–0.28±0.76	–1.61±0.11	–0.54±0.40	1.55±0.35
TbU	–0.49±0.20	–1.32±0.17	–0.29±1.15	1.87±0.66	1.08±1.08	–1.57±0.10	–0.40±1.04	1.54±0.48
YaY	–0.81±0.18	–1.42±0.25	1.19±1.21	1.76±0.75	–0.08±0.90	–1.57±0.25	–0.56±0.10	1.59±0.37
ChU	–0.40±0.39	–1.46±0.07	0.52±1.51	1.74±0.40	–0.33±0.73	–1.58±0.40	–0.40±0.37	1.67±0.37
BoU	–0.40±0.35	–1.45±0.10	0.71±1.36	1.76±0.47	–0.48±0.62	–1.57±0.39	–0.44±0.36	1.66±0.37
SuG	0.33±0.44	–1.27±0.10	0.30±1.07	1.94±0.49	–0.45±1.25	–1.47±0.51	–0.10±0.72	1.75±0.33
BuO	–0.28±0.88	–1.32±0.08	0.22±1.17	1.82±0.50	–0.69±0.78	–1.52±0.45	–0.16±0.72	1.71±0.35
ZaG	–0.22±0.89	–1.23±0.06	0.03±1.01	1.82±0.63	–0.66±0.89	–1.54±0.49	–0.19±0.65	1.70±0.33
ZaD	–0.29±0.68	–1.17±0.14	0.11±0.86	1.93±0.69	–0.42±0.99	–1.60±0.51	–0.39±0.44	1.66±0.31